Nuclear organisation and replication timing are coupled through RIF1-PP1 interaction

Stefano Gnan [1,2,3], Ilya M. Flyamer [4,$], Kyle N. Klein [5,$], Eleonora Castelli [2,6], Jesse L. Turner [5], Patrick Weber [7], Andreas Maiser [8], Elin Enervald [1,2], Cristina M. Cardoso [7], Wendy A. Bickmore [4], David M. Gilbert [5] and Sara C. B. Buonomo [1,2,*]

1 Epigenetics & Neurobiology Unit, European Molecular Biology Laboratory (EMBL Rome), Monterotondo, Italy.
2 Institute of Cell Biology, School of Biological Sciences University of Edinburgh, Roger Land, Building, Alexander Crum Brown Road, Edinburgh, EH9 3FF, UK.
3 Current address: Institute Curie, CNRS UMR3244, Pavillon Trouillet-Rossignol, 26 Rue d'Ulm, 75005 Paris, France.
4 MRC Human Genetics Unit, Institute of Genetics and Molecular Medicine, University of Edinburgh, Crewe Road South, Edinburgh EH4 2XU, UK.
5 Department of Biological Science, Florida State University, Tallahassee, Florida 32306, USA.
6 Current address: Friedrich Miescher Institute for Biomedical Research, 4058 Basel, Switzerland.
7 Cell Biology and Epigenetics, Department of Biology, Technische Universität Darmstadt, 64287 Darmstadt, Germany.
8 Department of Biology II, LMU Munich, 81377 Munich, Germany.

[$]These authors contributed equally to the work
[*]Corresponding author and lead contact: sara.buonomo@ed.ac.uk

Keywords: replication timing, nuclear organisation, Rif1, replication foci, PP1

Abstract

Parallels between three-dimensional genome organisation and replication timing suggests the hypothesis of their possible interdependence. However, it remains unknown whether nuclear architecture overall plays an instructive role in the replication-timing program. Here we demonstrate that they are coupled through RIF1, the molecular hub that co-regulates both processes. Both nuclear organisation and replication timing depend upon the interaction between RIF1 and PP1. However, whereas nuclear architecture requires the full complement of RIF1 and its interaction with PP1, replication timing is not sensitive to RIF1 dosage. RIF1's role in replication timing also extends beyond its interaction with PP1. Availing of this separation-of-function approach, we have therefore identified the molecular bases of the co-dependency of the replication-timing program and nuclear architecture.

Introduction

In eukaryotes, origins of DNA replication are not activated all at once. Origin firing follows a cell-type specific temporal program known as DNA replication timing. The replication-timing program is mirrored by the spatial distribution in the nucleus of replication foci, which are clusters of about 5 simultaneously activated bidirectional replication forks (Chagin et al., 2016). Both spatial and temporal replication patterns are re-established every cell cycle in G1, at the timing decision point (TDP) (Dimitrova and Gilbert, 1999), that coincides with the formation of chromosomal territories (Walter et al., 2003) and the re-establishment of chromatin architecture and interphase-nuclear configuration (Dileep et al., 2015; Nagano et al., 2017). The spatial organisation of DNA replication is evident at multiple levels. The units of DNA replication timing, replication domains (RD), coincide with one of the basic units of three-dimensional (3D) genome organisation, the topologically associated domains (TADs) (Pope et al., 2014). Recently, *in cis* elements (early replicating control elements-ERCEs) that can simultaneously influence chromatin looping and replication timing have also been identified (Sima et al., 2019). Moreover, the "assignment" of RDs as early or late replicating (the establishment of the replication-timing program), takes place on a chromosome-domain level, prior to the specification of the active origins of replication (Dimitrova and Gilbert, 1999). On a global scale, the early and late replicating genomes overlap with the A and B spatial compartments identified by Chromosome Conformation Capture methods (HiC) (Moindrot et al., 2012; Ryba et al., 2010; Yaffe et al., 2010) and are segregated in the nuclear interior or the periphery of the nucleus and nucleolus respectively. Finally, a recent study from budding yeast has shown that activation of early origins drives their internalisation (Zhang et al., 2019). However, no causal link between the temporal and spatial aspects of DNA replication organisation has been established.

RIF1 is a key genome-wide regulator of replication timing (Cornacchia et al., 2012; Foti et al., 2016; Hayano et al., 2012; Hiraga et al., 2014; Peace et al., 2014; Seller and O'Farrell, 2018; Yamazaki et al., 2012). It is also involved in re-establishing spatial chromatin organisation in the nucleus at G1 (Foti et al., 2016), and in the control of the spatial dynamics of replication foci (Cornacchia et al., 2012). RIF1 could therefore be a molecular connection between temporal and spatial organisation of DNA replication in mammalian cells.

The molecular function of RIF1 is still unclear, although this 266kD protein is involved in a variety of functions such as DNA repair (Buonomo et al., 2009; Chapman et al., 2013; Daley and Sung, 2013; Di Virgilio et al., 2013; Feng et al., 2013; Gupta et al., 2018; Hengeveld et al., 2015; Martina et al., 2014; Mirman et al., 2018; Noordermeer et al., 2018; Silverman et al., 2004; Spies et al., 2019), telomere length regulation in yeast (Gallardo et al., 2011; Hardy et al., 1992; Mattarocci et al., 2017; Shi et al., 2013; Teixeira et al., 2004), cytokinesis (Bhowmick et al., 2019), epigenetic (Daxinger et al., 2013; Li et al., 2017; Tanaka et al., 2016; Toteva et al., 2017; Zofall et al., 2016) and DNA replication-timing control. Mammalian RIF1 interacts with components of the nuclear lamina (Foti et al., 2016; Roux et al., 2012), behaving as an integral part of this insoluble nuclear scaffold and chromatin organiser. RIF1 associates with the late replicating genome, forming megabase-long domains called RIF1-associated-domains (RADs) (Foti et al., 2016). It is unknown what directs the association to chromatin, but both the N and C terminus of RIF1 have been shown to be capable of mediating interaction with DNA (Kanoh et al., 2015; Mattarocci et al., 2017; Moriyama et al., 2017; Moriyama et al., 2018; Sukackaite et al., 2014; Xu et al., 2010). No clear structure-function data are available, but RIF1 has a highly-conserved interaction with Protein Phosphatase 1 (PP1) (Alver et al., 2017; Dave et al., 2014; Fardilha et al., 2011; Guruharsha et al., 2011; Hiraga et al., 2014; Hiraga et al., 2017; Mattarocci et al., 2014; Moorhead et al., 2008; Sreesankar et al., 2015; Sreesankar et al., 2012; Trinkle-Mulcahy et al., 2006). According to data from yeast and mammalian cells, such interaction is critical to regulate the firing of individual, late origins of replication (Alver et al., 2017; Dave et al., 2014; Hiraga et al., 2014; Hiraga et al., 2017; Mattarocci et al., 2014). Activation of these

origins would be promoted by Rif1 removal in late S-phase, led by the increasing levels of cyclin-dependent Kinase (CDK) activity (Alver et al., 2017; Dave et al., 2014; Hiraga et al., 2014; Hiraga et al., 2017; Mattarocci et al., 2014; Seller and O'Farrell, 2018). These studies therefore place the role of the RIF1-PP1 interaction at the stage of execution of the replication-timing program, in S-phase. However, we have identified a role for RIF1 as a chromatin organiser earlier during the cell cycle, in G1 phase, around the time of the establishment of the replication-timing program (Foti et al., 2016). Rif1 deficiency impacts nuclear architecture, relaxing the constraints that normally limit chromatin interactions between domains with the same replication timing (Foti et al., 2016). It is unknown if Rif1-dependent chromatin architecture establishment affects the replication-timing program, how RIF1 contributes to nuclear organisation, and if and how the interaction with PP1 plays a role in this function. More generally, the functional relationship between nuclear architecture and replication timing is still unclear.

Here, we tackle this question by interfering with the RIF1-PP1 interaction. Our results show that both replication timing and nuclear organisation depend upon RIF1-PP1 interaction. However, unlike the replication-timing program, we have discovered that nuclear organisation is exquisitely sensitive to RIF1's dosage. Using this separation-of-function approach, we have identified in RIF1 the molecular hub for their co-regulation. In addition, we have shown that the replication-timing program can be established and executed independent of the 3D architecture of chromatin contacts or the spatial distribution of replication foci, as long as there is some RIF1 present.

Results

Mouse embryonic stem cells expressing *Rif1*$^{\Delta PP1}$

RIF1-PP1 interaction promotes the continuous dephosphorylation of MCM4, bound to origins that are "marked" to be activated only during the later part of S-phase (Alver et al., 2017; Dave et al., 2014; Hiraga et al., 2014; Hiraga et al., 2017; Mattarocci et al., 2014). This suggests that, through RIF1, PP1 contributes to the control of the timing of firing of individual origins of replication. However, the functional significance of RIF1-PP1 interaction in the general context of the establishment and domain-level regulation of the replication-timing program, and in the context of nuclear 3D organisation is unknown. Therefore, mutations that interfere with RIF1-PP1 interaction are potential tools to achieve separation-of-function between nuclear organisation and replication timing.

We have recently identified the sites within RIF1 that mediate the physical contacts with PP1 (SILK and RVSF motifs, residues 2128–2131 and 2150–2153). As point mutations of the interface residues reduce the interaction to undetectable levels (RIF1$^{\Delta PP1}$: SILK into SAAA and RVSF into RVSA, Sukackaite et al., 2017), we sought to express the *Rif1*$^{\Delta PP1}$ mutant in mESCs. However, *Rif1* overexpression is toxic and therefore, in order to create a system to expresses *Rif1*$^{\Delta PP1}$ in a physiological context, we have utilised *Rif1*$^{FH/flox}$ mESCs. In these cells, one allele of *Rif1* contains loxP sites flanking exons 5 to 7 ((Buonomo et al., 2009), *Rif1*^{flox}), while the second is a knock-in of a FLAG-HA2 tag (FH) into the *Rif1* locus (*Rif1*^{FH}) ((Cornacchia et al., 2012), Fig. S1A and B). We have targeted the FH allele with a mini-gene encoding *Rif1*$^{\Delta PP1}$. As a control, following the same strategy, we have also knocked-in a *Rif1* wild type mini-gene (*Rif1*^{TgWT}). Thus, Cre-mediated deletion of the *Rif1*^{flox} allele leaves FH-tagged *Rif1*$^{\Delta PP1}$, *Rif1*^{TgWT} or the parental *Rif1*^{FH} alleles as the sole source of RIF1, effectively creating inducible FH-tagged *Rif1* hemizygous cells. Upon tamoxifen-mediated Cre recombination, we have therefore studied the consequences of abolishing RIF1-PP1 interaction in *Rif1*$^{\Delta PP1/flox}$ (*Rif1*$^{\Delta PP1/-}$, abbreviated Rif1-ΔPP1) and used as controls *Rif1*$^{TgWT/flox}$ and the parental cell line *Rif1*$^{FH/flox}$ (*Rif1*$^{TgWT/-}$ and *Rif1*$^{FH/-}$, abbreviated respectively Rif1-TgWT and Rif1-FH). In agreement with the fact that, upon Cre induction, all the Rif1 FH-tagged alleles are hemizygous, RIF1-ΔPP1,

RIF1-TgWT and RIF1-FH, are expressed at comparable levels (Fig. 1A, B and C). We next checked RIF1 chromatin association in Rif1-ΔPP1 and Rif1-TgWT cell lines. In *Drosophila* embryos, it was shown that CDK-dependent phosphorylation of the residues adjacent to the PP1-interacting motif, inhibits RIF1 association to chromatin (Seller and O'Farrell, 2018). In principle, the level of phosphorylation of these residues could be controlled by RIF1-associated PP1, maintaining them dephosphorylated until late S-phase, when CDK activity is sufficiently high to overcome the action of the phosphatase. Consequently, disrupting the interaction between RIF1 and PP1 could interfere with the dynamics of RIF1 association to the chromatin. However, in both Rif1-ΔPP1 and Rif1-TgWT cell lines, we found that RIF1 displays a comparable degree of chromatin-association (Fig. 1D). These data suggest that the interaction with PP1 is therefore not essential for regulating RIF1 dynamics.

RIF1 deficiency in mESCs affects nuclear function at multiple levels. In order to dissect which of RIF1's functions is mediated through PP1, we have compared Rif1-ΔPP1 to *Rif1*$^{-/-}$ (Rif1-KO) mESCs. One of the features of Rif1-KO cells is the doubling of the population in G2, accompanied by a decreased S-phase population (Fig. 1E and (Foti et al., 2016)). Our data show that *Rif1* hemizygosis (Rif1-FH and Rif1-TgWT) results in an altered cell cycle similar to RIF1 deficiency (Fig. 1E). Importantly, cell cycle-distribution in both Rif1-ΔPP1 and Rif1-TgWT cell lines appears comparable to Rif1-FH cells. These results suggest that the defective cell cycle progression of *Rif1* null cells is not attributable to altered PP1 function but to insufficient levels of RIF1. Another consequence of loss of Rif1 function in mESCs is the alteration of the gene expression profile (Foti et al., 2016), including the de-repression of MERVLs (Li et al., 2017), an effect that RIF1 shares with other epigenetic and DNA replication regulators (Yang et al., 2015). We therefore compared the level of MERVL RNA in Rif1-WT, Rif1-KO, Rif1-TgWT and Rif1-ΔPP1 cells. After four days of deletion, MERVLs are upregulated not only in Rif1-ΔPP1 and Rif1-KO cells, but, surprisingly, also in the hemizygous controls (Fig. 1F), suggesting that, as for cell cycle progression, gene expression control is also sensitive to RIF1 dosage.

RIF1-PP1 interaction is important to organise the replication-timing program

The most conserved function of RIF1 is the control of the replication-timing program and Rif1-KO cells show pronounced genome-wide changes of the temporal program of origin firing (Cornacchia et al., 2012; Foti et al., 2016). As RIF1-PP1 interaction has been shown to be important, at least during the execution of the replication-timing program in S-phase, (Alver et al., 2017; Dave et al., 2014; Hiraga et al., 2014; Hiraga et al., 2017; Mattarocci et al., 2014), expression of *Rif1*$^{\Delta PP1}$ should affect replication timing to a similar extent to *Rif1* deletion. In agreement with this prediction, hierarchical clustering of genome-wide replication timing shows that Rif1-ΔPP1 and Rif1-KO mESCs cluster together, while *Rif1*$^{+/+}$ (Rif1-WT) and control hemizygous (Rif1-FH and Rif1-TgWT) form a separate cluster (Fig. 2A). The replication profiles of both Rif1-ΔPP1 and Rif1-KO mESCs appear similarly compressed around the zero (Fig. 2B), suggesting an analogous loss of temporal control of origin firing. In both cases, a comparable fraction of the genome displays replication timing switches and changes (Fig. S2A). Importantly, the replication timing changes induced by the expression of *Rif1*$^{\Delta PP1}$ are not attributable to Rif1 haploinsufficiency. In fact, the replication-timing profiles of Rif1 hemizygous controls (Rif1-FH and Rif1-TgWT), are very similar to the wild type cells (Rif1-WT, Fig. 2B and C). Despite the similarities, however, the impact of loss of RIF1 versus loss of RIF1-PP1 interaction on the replication-timing program is not identical. *Rif1*$^{\Delta PP1}$ expressing cells maintain a better degree of distinction between earlier and later replicating domains than Rif-KO (Fig. 2B, C and Fig. S2B). These data suggest that RIF1-dependent control of the replication-timing program is not entirely exerted through PP1 and some other function of RIF1 partially contributes as well.

DNA replication timing is independent of the spatial distribution of replication foci

DNA replication takes place in a spatially organised manner (Nakamura et al., 1986; Nakayasu and Berezney, 1989), with the distribution of replication foci correlated to the time of replication (Fox et al., 1991). In support of the view that these two features of DNA replication are inter-dependent, we have shown that in mouse primary embryonic fibroblasts (pMEFs), RIF1 deficiency induces changes of both spatial distribution of replication foci and replication timing (Cornacchia et al., 2012). Unlike Rif1-KO, Rif1-ΔPP1 cells partially retain the distinction between early and late replicating domains. This difference could be explained if PP1 was not required for the 3D organisation of replication foci. However, Rif1-ΔPP1 cells show an aberrant distribution of replication foci highly comparable to *Rif1* null cells (Fig. 2D). Moreover, similarly to what happens in Rif1-KO cells, expression of *Rif1*$^{\Delta PP1}$ does not induce accumulation in early S-phase, as judged from the analysis of DNA content (Fig. S2C). Therefore, the increase in early-like replication foci patterns is due to a perturbed spatial organisation of the replication foci, that leads to their misclassification. The cells that show an early-like pattern display many replication foci throughout the nucleoplasm (Fig. S3A). This configuration could be achieved either by an overall increase in the number of replication forks or by their de-clustering, meaning that the number of forks per replication focus could be decreased, especially within the larger, mid-late replication foci. The first hypothesis seems unlikely, as the number of active forks depends on the abundance of limiting factors (Mantiero et al., 2011). We have therefore employed 3D-SIM to study the effect of *Rif1* deficiency or expression of *Rif1*$^{\Delta PP1}$ on the total number of replication forks and their clustering, by matching the total number of replication forks to the number of replication foci. Ideally, we should have analysed separately early, mid and late S-phase, as we would expect that a non-functional RIF1 would preferentially cause de-clustering of mid and late S-phase foci. However, since RIF1 deletion and expression of *Rif1*$^{\Delta PP1}$ induce a loss of equivalence between replication foci distribution and replication timing, this distinction was impossible. Our approach is therefore bound to cause an under-estimation of any effect. As expected, RIF1 deficiency or expression of *Rif1*$^{\Delta PP1}$ do not alter the total number of replication forks per nucleus (Fig. S3B). However, they cause a decrease of the number of replication forks per replication focus (Fig. S3C), supporting the idea that the apparent increase of early S-phase like pattern is due to a de-clustering of replication foci. In conclusion, the maintenance of a basic degree of distinction between early and late replicating regions in Rif1-ΔPP1 cannot be explained by a retention of replication foci spatial organisation. Very interestingly, our analysis indicates that Rif1 hemizygosis (Rif1-hem=Rif-FH+Rif1-TgWT) affects the spatial distribution of replication foci too (Fig. 2D). As these cells do not have any measurable perturbation of their replication-timing program, these results suggest that spatial distribution of replication foci and the timing of replication can be uncoupled.

RIF1 dosage is important for the compartmentalisation of chromatin contacts

The distribution of replication foci in the nucleus reflects a stable organisation of chromatin that is maintained until metaphase. To gain a more comprehensive understanding of chromatin organisation, we analysed nuclear architecture in Rif1-KO, Rif1-ΔPP1 and Rif1 hemizygous cells by HiC. We have previously shown by 4C that RIF1 deficiency induces an increase of low-frequency contacts between TADs with different replication timing (Foti et al., 2016). In agreement with these previous results, our HiC data indicate that *Rif1* deletion increases the contacts between TADs *in cis* (Rif1-WT and Rif1-KO, Fig. 3A), especially at long range (Fig. 3B, Fig. S4A, B and C). The contacts gained preferentially involve late-replicating TADs interacting with early-replicating (Fig. 3C, Fig. 4A, left) and RIF1-enriched gaining contacts with RIF1-poor TADs (Rif1-WT and Rif1-KO, Fig. 4A, right). These changes cannot be explained by the increased fraction of cells in G2 in Rif1-KO and Rif1-ΔPP1 cells, as it was shown that chromosome compaction in G2/M favours the establishment of short-

range interactions (Nagano et al., 2017). They suggest instead the possible alteration of the A/B compartmentalisation in mutant cells compared with Rif1-WT ESC's (Fig. 4B). In agreement with previous data that have reported a more "open chromatin" (Cornacchia et al., 2012; Foti et al., 2016; Yamazaki et al., 2012), *Rif1*'s loss of function induces an expansion of the A compartment (Fig. 4C). Loss of RIF1-PP1 interaction induces alterations of chromatin organisation comparable to Rif1-KO (Fig. 4B), with a similar degree of expansion of the A compartment (Fig. 4C). The proportion of the genome that shows genomic positions switching compartments is highly comparable between *Rif1* null and Rif1-ΔPP1 cells (Fig. 4D and Fig. S4D). This supports the conclusion that PP1 plays a key role in RIF1-dependent control of chromatin organisation.

Unexpectedly, chromatin architecture in *Rif1* hemizygous cells (Rif1-FH and Rif1-TgWT) shows an intermediate but reproducible degree of change, although not statistically significant. Halving *Rif1* dosage, is sufficient to induce a gain of *in cis* contacts between TADs of opposite replication timing (Fig. 3A, B and C), especially evident in the long-range contacts (Fig. S4A and B). Accordingly, the overall A/B compartment organisation in Rif1-TgWT and Rif1-FH cells clusters together with *Rif1* null and Rif1-ΔPP1 cells (Fig. 4B), with an expansion of the A compartment that is intermediate between Rif1-WT and Rif1-KO/Rif1-ΔPP1 cells (Fig. 4C). A similar fraction of the Rif1-TgWT population displays comparable compartment changes (Fig. 4D). These data indicate that chromatin architecture is exquisitely sensitive to RIF1 dosage, and that decreasing the levels of RIF1 induces a progressive alteration of nuclear organisation. This is in striking contrast with the effect of varying RIF1 levels on the regulation of replication timing.

Discussion

The remarkable coincidence of spatial distribution and replication timing of different portions of the genome, at multiple levels of organisation and throughout evolution, has encouraged the idea of a causal relationship between nuclear architecture and replication timing. At a molecular level, their covariation, for example during cell fate determination and embryonic development, finds a confirmation in their co-dependence on RIF1. In this work, we show that both aspects of nuclear function depend upon the interaction between RIF1 and PP1. However, 3D organisation of chromatin contacts and replication timing show a different degree of dependency on RIF1-PP1 interaction and are differentially influenced by RIF1's dosage. The loss of RIF1-PP1 interaction affects the compartmentalisation of chromatin contacts comparably to a complete loss of RIF1 function, while it only partially recapitulates the effects of *Rif1*$^{-/-}$ on the control of replication timing. In addition, the former is sensitive to RIF1's dosage, while *Rif1's* haploinsufficiency does not affect the latter.

RIF1 is known to multimerise (Kobayashi et al., 2019; Moriyama et al., 2018; Xu et al., 2010) and to interact with the nuclear lamina (Foti et al., 2016; Roux et al., 2012). RIF1 multimers could act as a sub-stochiometric platform, interacting with different regulators of replication timing, in addition to PP1. In this case, the consequences of the complete loss of RIF1 function on the replication-timing program would amount to the sum of perturbation of multiple pathways that control the timing of origin activation. For example, RIF1-ΔPP1 may only specifically interfere with the PP1-dependent control of DDK activity at origins, while other RIF1 interactors may contribute to the epigenetic control of origin activation. The proteins associated with RIF1 are enriched for chromatin and epigenetic regulators (Sukackaite et al., 2017), and the contribution of histone modifiers to the control of replication timing has long been recognised (Jorgensen et al., 2007; Li et al., 2005; Takebayashi et al., 2013; Vogelauer et al., 2002; Yokochi et al., 2009; Yoshida et al., 2014). However, an understanding of the effect of *Rif1* deletion on the epigenetic landscape is still missing, leaving this hypothesis currently hard to test (Cornacchia et al., 2012; Dan et al., 2014; Foti et al., 2016; Li et al., 2017). In the context of chromatin architecture organisation, RIF1 multimers could

directly participate in the creation of local scaffolds that restrict chromatin mobility or, alternatively, could regulate other proteins with this role. In either case, a reduction of RIF1 dosage could have structural, quantitative consequences.

Our results identify RIF1 as a molecular link, a point of convergence and co-regulation. We propose that RIF1, specifically, and not generic nuclear architecture, coordinates the replication-timing program with nuclear 3D organisation. In agreement with this view, recent data show that cohesins and CTCF are not involved in the regulation of replication timing (Oldach and Nieduszynski, 2019; Sima et al., 2019). Altogether, these data suggest that replication timing and nuclear architecture, or at least 3D organisation of chromatin contacts and spatial distribution of replication foci, are not linked by a causative relationship. Yet, they are coregulated, both during cell cycle and embryonic development, and RIF1 is a point of convergence. Having established this, is an important step to start addressing the fundamental question of why this coordination is important. During embryonic development in different organisms, for example in *Drosophila melanogaster*, replication timing (Seller and O'Farrell, 2018) and TADs definition both emerge around the time when zygotic transcription starts (Ogiyama et al., 2018). Could uncoupling these two events have consequences on gene expression? We can alter chromatin organisation, leaving replication timing intact, by halving RIF1 dosage. This affects cell cycle progression and the repression of MERVLs (this work). In a complementary approach, it has been shown that alteration of replication timing by overexpression of limiting replication factors during early *Xenopus laevis* development, that presumably leaves nuclear architecture intact, affects the onset of zygotic transcription and the transition into gastrulation (Collart et al., 2013). It is therefore tempting to speculate that the covariation of replication timing and nuclear architecture could be important to coordinate gene expression and the choice of origins of replication.

Acknowledgments

We would like to acknowledge Martin Waterfall from the IIIR Flow Cytometry Core Facility, University of Edinburgh; David Kelly from the COIL facility, WTCCB, University of Edinburgh; Vladimir Benes and the Genomic Core Facility at EMBL Heidelberg; Philip Hublitz from Gene expression Facility, EMBL Monterotondo; Violetta Parimbeni for mouse husbandry, EMBL Monterotondo. SG was funded by ERC consolidator award 726130 to SCBB; EC was supported by the Erasmus Program. EE received funding from the European Union's Horizon 2020 research and the Marie Skłodowska-Curie Individual Fellowship grant agreement No. 660985 and from the ERC consolidator award

726130 to SCBB. IMF was funded by the Darwin Trust of Edinburgh. SCBB thanks the ERC, DMG thanks NIH grant GM083337, W.A.B is funded by a Medical Research Council University Unit programme grant [MC_ UU_00007/2]

Author Contributions

SG has created the cellular system, performed the majority of the experiments and the bioinformatics analysis. IF has helped with HiC experiments and analysis. KK and JT have performed

the replication timing measures. EC has stained and scored with SG replication-timing patterns. PW and AM have respectively stained cells, acquired 3D-SIM images and performed the analysis. EE has analysed MERVL expression. WAB, DMG, CMC have supported the work with personnel, resources, scientific discussions and critical reading of the manuscript. SCBB has conceived the project, performed some of the experiments and written the manuscript.

Declaration of Interests

The authors declare no competing interests.

Figure Legends

Figure 1. **The levels of expression and association to chromatin of RIF1-TgWT and RIF1-ΔPP1 are comparable to the levels detected in *Rif1* hemizygous cells.**

A. Western blot analysis of RIF1 levels after four days of hydroxytamoxifen treatment, to induce Cre-mediated deletion of $Rif1^{flox}$ allele. Proteins were extracted from untagged Rif1-WT ($Rif1^{+/+}$); Rif1-KO ($Rif1^{flox/flox}$); FLAG-HA2(FH) knock-in tagged Rif1 hemizygous: Rif1-FH ($Rif1^{FH/flox}$); FH-tagged targeted Rif1-TgWT hemizygous ($Rif1^{TgWT/flox}$); FH- tagged targeted Rif1-ΔPP1 hemizygous ($Rif1^{\Delta PP1/flox}$). Anti-mouse Rif1 polyclonal rabbit antibody 1240 (anti-RIF1) was used to detect both FH-tagged and untagged proteins. Mouse ascites 16B12 (anti-HA) detects only FH-tagged Rif1. SMC1 levels were used as loading control.
B. Quantitative analysis of total levels of FH-tagged RIF1, measured by intra-cellular FACS staining. Anti-HA mouse ascities 16B12 was used to stain the indicated cell lines. $Rif1^{FH/FH}$= homozygous knock-in FH-tagged RIF1, as control of quantitative staining. The plot shows distributions of densities from HA signal, measured in arbitrary units. One representative experiment is shown.
C. Quantification from Fig. 1B. The bar plot represents the median intensities for the experiment shown and the error bars indicate 95% confidence intervals.
D. Quantitative analysis of the levels of chromatin-associated FH-tagged RIF1 throughout cell cycle (one representative experiment), measured by FACS staining. Cytoplasmic and nucleoplasmic proteins were pre-extracted before fixing chromatin-associated proteins. Anti-HA mouse ascites 16B12 was used to visualize FH-tagged Rif1 as in B. Cell cycle stage was determined by DNA quantification (DAPI staining).
E. Cell cycle distribution of the indicated cell lines, as determined by FACS quantitation of EdU incorporation (S-phase) and DAPI staining (DNA amount). The average value of three independent clones per genotype is shown. Average of three experiments. Error bars indicate the standard deviation. *P* values are calculated using Wilcox test.
F. Quantification by qRT-PCR of MERVL's upregulation in the indicated genotypes, expressed as fold increase over MERVL levels in the same cell lines, before Cre induction. GAPDH was used to normalize. One representative experiment is shown and displays the average of 3 biological replicates for Rif1-ΔPP1 and Rif1-TgWT, 2 for Rif1-KO and one reference for Rif1-WT. Error bars indicate standard deviations.

Figure 2. **Effect of loss of RIF1-PP1 interaction on the replication-timing program and on the spatial distribution of replication foci.**

A. Hierarchical cluster analysis of Pearson correlation coefficient of genome-wide replication-timing (RT) profiles between replicas, bin size 50kb. The analysis shows preferential clustering of RT distribution from Rif1-KO and Rif1-ΔPP1 lines, while RT distribution from Rif1-WT clusters with Rif1-TgWT and Rif1-FH lines.
B. Representative RT profile from Chromosome 17. The solid line shows the average of three biological replicas, except for Rif1-FH (single, parental clone). RT scores are calculated as the $\log_2$ of the ratio between mapped reads in the early and late replicating fractions of the cell cycle over bins of 50Kb.
C. Genome-wide distribution of 50kb genomic windows on the bases of their RT scores. Average of three independent lines per genotype is shown, except for Rif1-FH. Shades represents standard deviations. RT scores from Rif1-WT and Rif1 hemizygous lines (Rif1-TgWT and Rif1-FH) show a bimodal distribution, defining distinct early and late genomic regions. On the contrary, the distribution of RT scores from Rif1-KO lines shows a tendency towards a unimodal distribution, centered around zero. Rif1-ΔPP1 lines display an increase of the windows with RT=0, but still a bimodal distribution of the RT values.
D. The spatial distribution of replication foci (replication patterns) was visualized by EdU and DAPI staining. Cells were pulsed for 30 minutes with EdU and fixed. Examples in Fig. S3A. Pie charts show the relative distribution of S-phase cells (EdU positive) between replication patterns corresponding to early, mid and late S-phase. For each genotype, three independent lines and two separate

experiments were blind-scored. As Rif-FH cells are a single cell line with no biological replicas (parental) and the results are very similar to the results from Rif1-TgWT, they were pooled (Rif1-hem). In the table, statistically significant differences are summarized. *P* values are calculated by χ^2 test.

Figure 3. **RIF1 spatially confines chromatin contacts in a dose-dependent manner.**

A. Quantification of genome-wide inter-TADs *in cis* chromatin contacts (arbitrary units). Each clone is represented by a smaller circle. The mean from three independent clones per genotype is indicated by the bigger circle, except for the parental line Rif1-FH. *P* values calculated by Wilcox test.
B. Representative distribution of the median number of *in cis* chromatin contacts per indicated position (arbitrary units) within the specified region of Chromosome 17. Three independent clones per genotype were used. Upper: $\log_2$(balanced HiC signals). Lower: $\log_2$ ((balanced HiC signals (indicated line/Rif1-WT)). Red indicates a gain of interactions over Rif1-WT, while purple represents a loss. Saturated signals are shown. Heatmaps showing unsaturated signals in Fig. S4C.
C. Mean change of the number of *in cis* inter-TAD contacts expressed as percentage versus Rif1-WT, classified by RT score of the anchor and interacting TADs. Error bars indicate the error propagation of the standard deviations of each sample.

Figure 4. **Segregation of A and B nuclear compartments is sensitive to Rif1 dosage.**

A. Log2 ratio of the median number of contacts between pair of TADs, for three biological replicates per each indicated genotype, versus three biological replicates for Rif1-WT. On the left, TADs are divided on the basis of their RT, leading to the classification of chromatin contacts within or across RT. On the right, the same was done dividing the TADs on the basis of their association with Rif1 or of lack of thereof. The cut-off used for the fold change is +/- 1.5. Color scale has been saturated in order to facilitate the observation.
B. Pearson correlation of A/B compartmentalisation z at the resolution of 50Kb and hierarchical cluster analysis (Euclidean distance). A/B compartments calculated from Rif1-WT lines cluster alone, while from all other individual lines group in a single, separate cluster.
C. Distribution of genomic regions of 50kb windows between the A and B compartment. Average of three biological replicates is shown, but for the parental line Rif1-FH.
D. Percentage of 50kb-windows changing compartment in comparison to Rif1-WT lines, calculated for increasing thresholds (ΔAB). AtoB= windows changing assignment from the A to the B compartment (from a positive to a negative eigenvector value, passing the zero); towards A= windows within B compartment acquiring an eigenvector value less negative (closer to the zero); BtoA= windows changing assignment from the B to the A compartment (from a negative to a positive eigenvector value, passing the zero); towards B= windows within A compartment acquiring an eigenvector value less positive (closer to the zero).

References

Alver, R.C., Chadha, G.S., Gillespie, P.J., and Blow, J.J. (2017). Reversal of DDK-Mediated MCM Phosphorylation by Rif1-PP1 Regulates Replication Initiation and Replisome Stability Independently of ATR/Chk1. Cell Rep *18*, 2508-2520.

Bhowmick, R., Thakur, R.S., Venegas, A.B., Liu, Y., Nilsson, J., Barisic, M., and Hickson, I.D. (2019). The RIF1-PP1 Axis Controls Abscission Timing in Human Cells. Curr Biol *29*, 1232-1242 e1235.

Buonomo, S.B., Wu, Y., Ferguson, D., and de Lange, T. (2009). Mammalian Rif1 contributes to replication stress survival and homology-directed repair. The Journal of cell biology *187*, 385-398.

Chagin, V.O., Casas-Delucchi, C.S., Reinhart, M., Schermelleh, L., Markaki, Y., Maiser, A., Bolius, J.J., Bensimon, A., Fillies, M., Domaing, P*., et al.* (2016). 4D Visualization of replication foci in mammalian cells corresponding to individual replicons. Nat Commun *7*, 11231.

Chapman, J.R., Barral, P., Vannier, J.B., Borel, V., Steger, M., Tomas-Loba, A., Sartori, A.A., Adams, I.R., Batista, F.D., and Boulton, S.J. (2013). RIF1 is essential for 53BP1-dependent nonhomologous end joining and suppression of DNA double-strand break resection. Molecular cell *49*, 858-871.

Collart, C., Allen, G.E., Bradshaw, C.R., Smith, J.C., and Zegerman, P. (2013). Titration of four replication factors is essential for the Xenopus laevis midblastula transition. Science (New York, NY *341*, 893-896.

Cornacchia, D., Dileep, V., Quivy, J.P., Foti, R., Tili, F., Santarella-Mellwig, R., Antony, C., Almouzni, G., Gilbert, D.M., and Buonomo, S.B. (2012). Mouse Rif1 is a key regulator of the replication-timing programme in mammalian cells. The EMBO journal *31*, 3678-3690.

Daley, J.M., and Sung, P. (2013). RIF1 in DNA break repair pathway choice. Molecular cell *49*, 840-841.

Dan, J., Liu, Y., Liu, N., Chiourea, M., Okuka, M., Wu, T., Ye, X., Mou, C., Wang, L., Wang, L*., et al.* (2014). Rif1 maintains telomere length homeostasis of ESCs by mediating heterochromatin silencing. Dev Cell *29*, 7-19.

Dave, A., Cooley, C., Garg, M., and Bianchi, A. (2014). Protein Phosphatase 1 Recruitment by Rif1 Regulates DNA Replication Origin Firing by Counteracting DDK Activity. Cell Rep *7*, 53-61.

Daxinger, L., Harten, S.K., Oey, H., Epp, T., Isbel, L., Huang, E., Whitelaw, N., Apedaile, A., Sorolla, A., Yong, J*., et al.* (2013). An ENU mutagenesis screen identifies novel and known genes involved in epigenetic processes in the mouse. Genome Biol *14*, R96.

Di Virgilio, M., Callen, E., Yamane, A., Zhang, W., Jankovic, M., Gitlin, A.D., Feldhahn, N., Resch, W., Oliveira, T.Y., Chait, B.T*., et al.* (2013). Rif1 prevents resection of DNA breaks and promotes immunoglobulin class switching. Science (New York, NY *339*, 711-715.

Dileep, V., Ay, F., Sima, J., Vera, D.L., Noble, W.S., and Gilbert, D.M. (2015). Topologically associating domains and their long-range contacts are established during early G1 coincident with the establishment of the replication-timing program. Genome Res *25*, 1104-1113.

Dimitrova, D.S., and Gilbert, D.M. (1999). The spatial position and replication timing of chromosomal domains are both established in early G1 phase. Molecular cell *4*, 983-993.

Fardilha, M., Esteves, S.L., Korrodi-Gregorio, L., Vintem, A.P., Domingues, S.C., Rebelo, S., Morrice, N., Cohen, P.T., da Cruz e Silva, O.A., and da Cruz e Silva, E.F. (2011). Identification of the human testis protein phosphatase 1 interactome. Biochem Pharmacol *82*, 1403-1415.

Feng, L., Fong, K.W., Wang, J., Wang, W., and Chen, J. (2013). RIF1 counteracts BRCA1-mediated end resection during DNA repair. The Journal of biological chemistry *288*, 11135-11143.

Foti, R., Gnan, S., Cornacchia, D., Dileep, V., Bulut-Karslioglu, A., Diehl, S., Buness, A., Klein, F.A., Huber, W., Johnstone, E.*, et al.* (2016). Nuclear Architecture Organized by Rif1 Underpins the Replication-Timing Program. Molecular cell *61*, 260-273.

Fox, M.H., Arndt-Jovin, D.J., Jovin, T.M., Baumann, P.H., and Robert-Nicoud, M. (1991). Spatial and temporal distribution of DNA replication sites localized by immunofluorescence and confocal microscopy in mouse fibroblasts. Journal of cell science *99 (Pt 2)*, 247-253.

Gallardo, F., Laterreur, N., Cusanelli, E., Ouenzar, F., Querido, E., Wellinger, R.J., and Chartrand, P. (2011). Live cell imaging of telomerase RNA dynamics reveals cell cycle-dependent clustering of telomerase at elongating telomeres. Molecular cell *44*, 819-827.

Gupta, R., Somyajit, K., Narita, T., Maskey, E., Stanlie, A., Kremer, M., Typas, D., Lammers, M., Mailand, N., Nussenzweig, A.*, et al.* (2018). DNA Repair Network Analysis Reveals Shieldin as a Key Regulator of NHEJ and PARP Inhibitor Sensitivity. Cell *173*, 972-988 e923.

Guruharsha, K.G., Rual, J.F., Zhai, B., Mintseris, J., Vaidya, P., Vaidya, N., Beekman, C., Wong, C., Rhee, D.Y., Cenaj, O.*, et al.* (2011). A protein complex network of Drosophila melanogaster. Cell *147*, 690-703.

Hardy, C.F., Sussel, L., and Shore, D. (1992). A RAP1-interacting protein involved in transcriptional silencing and telomere length regulation. Genes & development *6*, 801-814.

Hayano, M., Kanoh, Y., Matsumoto, S., Renard-Guillet, C., Shirahige, K., and Masai, H. (2012). Rif1 is a global regulator of timing of replication origin firing in fission yeast. Genes & development *26*, 137-150.

Hengeveld, R.C., de Boer, H.R., Schoonen, P.M., de Vries, E.G., Lens, S.M., and van Vugt, M.A. (2015). Rif1 Is Required for Resolution of Ultrafine DNA Bridges in Anaphase to Ensure Genomic Stability. Dev Cell *34*, 466-474.

Hiraga, S., Alvino, G.M., Chang, F., Lian, H.Y., Sridhar, A., Kubota, T., Brewer, B.J., Weinreich, M., Raghuraman, M.K., and Donaldson, A.D. (2014). Rif1 controls DNA replication by directing Protein Phosphatase 1 to reverse Cdc7-mediated phosphorylation of the MCM complex. Genes & development *28*, 372-383.

Hiraga, S.I., Ly, T., Garzon, J., Horejsi, Z., Ohkubo, Y.N., Endo, A., Obuse, C., Boulton, S.J., Lamond, A.I., and Donaldson, A.D. (2017). Human RIF1 and protein phosphatase 1 stimulate DNA replication origin licensing but suppress origin activation. EMBO Rep *18*, 403-419.

Jorgensen, H.F., Azuara, V., Amoils, S., Spivakov, M., Terry, A., Nesterova, T., Cobb, B.S., Ramsahoye, B., Merkenschlager, M., and Fisher, A.G. (2007). The impact of chromatin modifiers on the timing of locus replication in mouse embryonic stem cells. Genome Biol *8*, R169.

Kanoh, Y., Matsumoto, S., Fukatsu, R., Kakusho, N., Kono, N., Renard-Guillet, C., Masuda, K., Iida, K., Nagasawa, K., Shirahige, K.*, et al.* (2015). Rif1 binds to G quadruplexes and suppresses replication over long distances. Nature structural & molecular biology *22*, 889-897.

Kobayashi, S., Fukatsu, R., Kanoh, Y., Kakusho, N., Matsumoto, S., Chaen, S., and Masai, H. (2019). Both a Unique Motif at the C Terminus and an N-Terminal HEAT Repeat Contribute to G-Quadruplex Binding and Origin Regulation by the Rif1 Protein. Molecular and cellular biology *39*.

Li, J., Santoro, R., Koberna, K., and Grummt, I. (2005). The chromatin remodeling complex NoRC controls replication timing of rRNA genes. The EMBO journal *24*, 120-127.

Li, P., Wang, L., Bennett, B.D., Wang, J., Li, J., Qin, Y., Takaku, M., Wade, P.A., Wong, J., and Hu, G. (2017). Rif1 promotes a repressive chromatin state to safeguard against endogenous retrovirus activation. Nucleic acids research *45*, 12723-12738.

Mantiero, D., Mackenzie, A., Donaldson, A., and Zegerman, P. (2011). Limiting replication initiation factors execute the temporal programme of origin firing in budding yeast. The EMBO journal *30*, 4805-4814.

Martina, M., Bonetti, D., Villa, M., Lucchini, G., and Longhese, M.P. (2014). Saccharomyces cerevisiae Rif1 cooperates with MRX-Sae2 in promoting DNA-end resection. EMBO Rep *15*, 695-704.

Mattarocci, S., Reinert, J.K., Bunker, R.D., Fontana, G.A., Shi, T., Klein, D., Cavadini, S., Faty, M., Shyian, M., Hafner, L*., et al.* (2017). Rif1 maintains telomeres and mediates DNA repair by encasing DNA ends. Nature structural & molecular biology *24*, 588-595.

Mattarocci, S., Shyian, M., Lemmens, L., Damay, P., Altintas, D.M., Shi, T., Bartholomew, C.R., Thoma, N.H., Hardy, C.F., and Shore, D. (2014). Rif1 Controls DNA Replication Timing in Yeast through the PP1 Phosphatase Glc7. Cell Rep *7*, 62-69.

Mirman, Z., Lottersberger, F., Takai, H., Kibe, T., Gong, Y., Takai, K., Bianchi, A., Zimmermann, M., Durocher, D., and de Lange, T. (2018). 53BP1-RIF1-shieldin counteracts DSB resection through CST- and Polalpha-dependent fill-in. Nature *560*, 112-116.

Moindrot, B., Audit, B., Klous, P., Baker, A., Thermes, C., de Laat, W., Bouvet, P., Mongelard, F., and Arneodo, A. (2012). 3D chromatin conformation correlates with replication timing and is conserved in resting cells. Nucleic acids research *40*, 9470-9481.

Moorhead, G.B., Trinkle-Mulcahy, L., Nimick, M., De Wever, V., Campbell, D.G., Gourlay, R., Lam, Y.W., and Lamond, A.I. (2008). Displacement affinity chromatography of protein phosphatase one (PP1) complexes. BMC Biochem *9*, 28.

Moriyama, K., Lai, M.S., and Masai, H. (2017). Interaction of Rif1 Protein with G-Quadruplex in Control of Chromosome Transactions. Advances in experimental medicine and biology *1042*, 287-310.

Moriyama, K., Yoshizawa-Sugata, N., and Masai, H. (2018). Oligomer formation and G-quadruplex binding by purified murine Rif1 protein, a key organizer of higher-order chromatin architecture. The Journal of biological chemistry *293*, 3607-3624.

Nagano, T., Lubling, Y., Varnai, C., Dudley, C., Leung, W., Baran, Y., Mendelson Cohen, N., Wingett, S., Fraser, P., and Tanay, A. (2017). Cell-cycle dynamics of chromosomal organization at single-cell resolution. Nature *547*, 61-67.

Nakamura, H., Morita, T., and Sato, C. (1986). Structural organizations of replicon domains during DNA synthetic phase in the mammalian nucleus. Experimental cell research *165*, 291-297.

Nakayasu, H., and Berezney, R. (1989). Mapping replicational sites in the eucaryotic cell nucleus. The Journal of cell biology *108*, 1-11.

Noordermeer, S.M., Adam, S., Setiaputra, D., Barazas, M., Pettitt, S.J., Ling, A.K., Olivieri, M., Alvarez-Quilon, A., Moatti, N., Zimmermann, M*., et al.* (2018). The shieldin complex mediates 53BP1-dependent DNA repair. Nature *560*, 117-121.

Ogiyama, Y., Schuettengruber, B., Papadopoulos, G.L., Chang, J.M., and Cavalli, G. (2018). Polycomb-Dependent Chromatin Looping Contributes to Gene Silencing during Drosophila Development. Molecular cell *71*, 73-88 e75.

Oldach, P., and Nieduszynski, C.A. (2019). Cohesin-Mediated Genome Architecture Does Not Define DNA Replication Timing Domains. Genes (Basel) *10*.

Peace, J.M., Ter-Zakarian, A., and Aparicio, O.M. (2014). Rif1 Regulates Initiation Timing of Late Replication Origins throughout the S. cerevisiae Genome. PLoS One *9*, e98501.

Pope, B.D., Ryba, T., Dileep, V., Yue, F., Wu, W., Denas, O., Vera, D.L., Wang, Y., Hansen, R.S., Canfield, T.K.*, et al.* (2014). Topologically associating domains are stable units of replication-timing regulation. Nature *515*, 402-405.

Roux, K.J., Kim, D.I., Raida, M., and Burke, B. (2012). A promiscuous biotin ligase fusion protein identifies proximal and interacting proteins in mammalian cells. The Journal of cell biology *196*, 801-810.

Ryba, T., Hiratani, I., Lu, J., Itoh, M., Kulik, M., Zhang, J., Schulz, T.C., Robins, A.J., Dalton, S., and Gilbert, D.M. (2010). Evolutionarily conserved replication timing profiles predict long-range chromatin interactions and distinguish closely related cell types. Genome Res *20*, 761-770.

Seller, C.A., and O'Farrell, P.H. (2018). Rif1 prolongs the embryonic S phase at the Drosophila mid-blastula transition. PLoS Biol *16*, e2005687.

Shi, T., Bunker, R.D., Mattarocci, S., Ribeyre, C., Faty, M., Gut, H., Scrima, A., Rass, U., Rubin, S.M., Shore, D.*, et al.* (2013). Rif1 and Rif2 shape telomere function and architecture through multivalent Rap1 interactions. Cell *153*, 1340-1353.

Silverman, J., Takai, H., Buonomo, S.B., Eisenhaber, F., and de Lange, T. (2004). Human Rif1, ortholog of a yeast telomeric protein, is regulated by ATM and 53BP1 and functions in the S-phase checkpoint. Genes & development *18*, 2108-2119.

Sima, J., Chakraborty, A., Dileep, V., Michalski, M., Klein, K.N., Holcomb, N.P., Turner, J.L., Paulsen, M.T., Rivera-Mulia, J.C., Trevilla-Garcia, C.*, et al.* (2019). Identifying cis Elements for Spatiotemporal Control of Mammalian DNA Replication. Cell *176*, 816-830 e818.

Spies, J., Lukas, C., Somyajit, K., Rask, M.B., Lukas, J., and Neelsen, K.J. (2019). 53BP1 nuclear bodies enforce replication timing at under-replicated DNA to limit heritable DNA damage. Nature cell biology *21*, 487-497.

Sreesankar, E., Bharathi, V., Mishra, R.K., and Mishra, K. (2015). Drosophila Rif1 is an essential gene and controls late developmental events by direct interaction with PP1-87B. Sci Rep *5*, 10679.

Sreesankar, E., Senthilkumar, R., Bharathi, V., Mishra, R.K., and Mishra, K. (2012). Functional diversification of yeast telomere associated protein, Rif1, in higher eukaryotes. BMC Genomics *13*, 255.

Sukackaite, R., Cornacchia, D., Jensen, M.R., Mas, P.J., Blackledge, M., Enervald, E., Duan, G., Auchynnikava, T., Kohn, M., Hart, D.J.*, et al.* (2017). Mouse Rif1 is a regulatory subunit of protein phosphatase 1 (PP1). Sci Rep *7*, 2119.

Sukackaite, R., Jensen, M.R., Mas, P.J., Blackledge, M., Buonomo, S.B., and Hart, D.J. (2014). Structural and Biophysical Characterization of Murine Rif1 C Terminus Reveals High Specificity for DNA Cruciform Structures. The Journal of biological chemistry.

Takebayashi, S., Lei, I., Ryba, T., Sasaki, T., Dileep, V., Battaglia, D., Gao, X., Fang, P., Fan, Y., Esteban, M.A.*, et al.* (2013). Murine esBAF chromatin remodeling complex subunits BAF250a and Brg1 are necessary to maintain and reprogram pluripotency-specific replication timing of select replication domains. Epigenetics Chromatin *6*, 42.

Tanaka, H., Muto, A., Shima, H., Katoh, Y., Sax, N., Tajima, S., Brydun, A., Ikura, T., Yoshizawa, N., Masai, H.*, et al.* (2016). Epigenetic Regulation of the Blimp-1 Gene (Prdm1) in B Cells Involves Bach2 and Histone Deacetylase 3. The Journal of biological chemistry *291*, 6316-6330.

Teixeira, M.T., Arneric, M., Sperisen, P., and Lingner, J. (2004). Telomere length homeostasis is achieved via a switch between telomerase- extendible and -nonextendible states. Cell *117*, 323-335.

Toteva, T., Mason, B., Kanoh, Y., Brogger, P., Green, D., Verhein-Hansen, J., Masai, H., and Thon, G. (2017). Establishment of expression-state boundaries by Rif1 and Taz1 in fission yeast. Proceedings of the National Academy of Sciences of the United States of America *114*, 1093-1098.

Trinkle-Mulcahy, L., Andersen, J., Lam, Y.W., Moorhead, G., Mann, M., and Lamond, A.I. (2006). Repo-Man recruits PP1 gamma to chromatin and is essential for cell viability. The Journal of cell biology *172*, 679-692.

Vogelauer, M., Rubbi, L., Lucas, I., Brewer, B.J., and Grunstein, M. (2002). Histone acetylation regulates the time of replication origin firing. Molecular cell *10*, 1223-1233.

Walter, J., Schermelleh, L., Cremer, M., Tashiro, S., and Cremer, T. (2003). Chromosome order in HeLa cells changes during mitosis and early G1, but is stably maintained during subsequent interphase stages. The Journal of cell biology *160*, 685-697.

Xu, D., Muniandy, P., Leo, E., Yin, J., Thangavel, S., Shen, X., Ii, M., Agama, K., Guo, R., Fox, D., 3rd*, et al.* (2010). Rif1 provides a new DNA-binding interface for the Bloom syndrome complex to maintain normal replication. The EMBO journal *29*, 3140-3155.

Yaffe, E., Farkash-Amar, S., Polten, A., Yakhini, Z., Tanay, A., and Simon, I. (2010). Comparative analysis of DNA replication timing reveals conserved large-scale chromosomal architecture. PLoS Genet *6*, e1001011.

Yamazaki, S., Ishii, A., Kanoh, Y., Oda, M., Nishito, Y., and Masai, H. (2012). Rif1 regulates the replication timing domains on the human genome. The EMBO journal *31*, 3667-3677.

Yang, B.X., El Farran, C.A., Guo, H.C., Yu, T., Fang, H.T., Wang, H.F., Schlesinger, S., Seah, Y.F., Goh, G.Y., Neo, S.P.*, et al.* (2015). Systematic identification of factors for provirus silencing in embryonic stem cells. Cell *163*, 230-245.

Yokochi, T., Poduch, K., Ryba, T., Lu, J., Hiratani, I., Tachibana, M., Shinkai, Y., and Gilbert, D.M. (2009). G9a selectively represses a class of late-replicating genes at the nuclear periphery. Proceedings of the National Academy of Sciences of the United States of America *106*, 19363-19368.

Yoshida, K., Bacal, J., Desmarais, D., Padioleau, I., Tsaponina, O., Chabes, A., Pantesco, V., Dubois, E., Parrinello, H., Skrzypczak, M.*, et al.* (2014). The histone deacetylases sir2 and rpd3 act on ribosomal DNA to control the replication program in budding yeast. Molecular cell *54*, 691-697.

Zhang, H., Petrie, M.V., He, Y., Peace, J.M., Chiolo, I.E., and Aparicio, O.M. (2019). Dynamic relocalization of replication origins by Fkh1 requires execution of DDK function and Cdc45 loading at origins. Elife *8*.

Zofall, M., Smith, D.R., Mizuguchi, T., Dhakshnamoorthy, J., and Grewal, S.I.S. (2016). Taz1-Shelterin Promotes Facultative Heterochromatin Assembly at Chromosome-Internal Sites Containing Late Replication Origins. Molecular cell *62*, 862-874.

START METHODS

Mouse embryonic stem cell derivation

Mouse embryonic stem cell (ESC) cells were derived as described in Foti et al, 2016, with the addition of 1 μM MEK inhibitor PD0325901 and 3 μM GSK3 inhibitor CH99021 (The University of Dundee, Dept. of Biochemistry, Medical Sciences Institute) in the culture media, from the start of the protocol.
Rif1$^{FH/flox}$ Rosa26$^{Cre-ERT/+}$ ESCs were derived by crossing Rif1$^{flox/+}$ Rosa26$^{Cre-ERT/Cre-ERT}$ (Buonomo et al, 2009) with Rif1$^{FH/FH}$ (Cornacchia et al, 2012) mice. The Rif1^{FH} allele was specifically targeted in the parental line Rif1$^{FH/flox}$ Rosa26$^{Cre-ERT/+}$ (Rif1-FH). Integrants were selected by hygromycin resistance. The targeting vector encodes for a codon-optimized cDNA of RIF1 (exon 8 to exon 36). Hygromycin-resistant colonies were screened for correct targeting of the Rif1^{FH} allele by Southern blot (EcoRV digest) and using a PCR-amplified probe (primers in Table 1).

Cell manipulation

ESCs were grown at 37°C in 7.5% CO_2 in Knockout DMEM (Gibco 10829-018), containing 12.5% heat-inactivated fetal bovine serum (Pan-Biotech), 1% non-essential amino acids (Gibco 11140-050), 1% Penicillin/Streptomycin (Gibco 15070063), 0.1 mM 2-Mercaptoethanol (Gibco 31350-010), 1% L-Glutamine (Gibco 25030-081), supplemented with 1 μM PD0325901 and 3 μM CH99021 and 20 ng/ml leukemia inhibitory factor (LIF, EMBL Protein Expression and Purification core facility).
Experiments were carried out each time from a frozen vial, at least two passages after thawing. $5.2 \cdot 10^6$ cells for Rif1-WT and $6.5 \cdot 10^6$ for Rif1-KO lines, per 15cm plate (or the equivalent for different size plates) were plated at day zero, when treatment with 200 nM 4-hydroxytamoxifen (OHT, Sigma H7904) started. Fresh medium with OHT was added after 48 hours. Cells were collected about 96 hours after starting OHT treatment.

Replication Timing analysis

Cells were pulsed for 2 hours with 10 μM BrdU, collected and fixed in ethanol 70%. Processing as described in (Ryba, Hiratani et al. 2011). Fastq files were aligned using Bowtie2 version 2.2.6 on mm10 as a reference genome. SAM files were converted into BAM files and sorted using Samtools version: 1.3.1. bamCompare version 3.1.3 was used to create bedgraph files with 50 kb and 1 kb binning of the $\log_2$ ratio of the early and late fraction. Duplicated reads were excluded from the computation of the bedgraph files. The two fractions were normalized based on the sequencing depth. XY chromosomes were excluded from the analysis. Plots and data manipulation was carried in R version 3.5.1. The original names of the cell lines used in these experiments, included in the name of the Repli-seq raw files are: RFHF14 = Rif1-FH, 14 tgWT A7 = Rif1-TgWT 1, 14 tgWT H4 = Rif1-TgWT 2, 14 tgwt H6 = Rif1-TgWT 3, 14 ΔP G11 = Rif1-ΔPP1 1, 14 ΔP H1 = Rif1-ΔPP1 2, 14 ΔP H2 = Rif1-ΔPP1 3, ESC B = Rif1-WT 1, ESC F = Rif1-WT 2, ESC H = Rif1-WT 3, ESC 5 = Rif1-KO 1, ESC 18 = Rif1-KO 2, ESC 24 = Rif1-KO 3.

Cell cycle distribution analysis

After four days of OHT treatment, cells were pulsed for 30 minutes with 10 µM EdU (Invitrogen A10044). Cells were then washed with cold DPBS (Thermo Fisher Scientific 14190094), collected, counted and fixed in EtOH 75%. Samples were kept at -20 °C for at least overnight. $7.5 \cdot 10^5$ cells were then processed for click-chemistry detection of EdU. After washing in cold DPBS, cells were permeabilised in DPBS/1% FBS/0.01 % Triton 100X (Sigma93426-250 mL) for 10 minutes on ice. After washing twice, cells were incubated in 900 µl of DPBS with 10 mM Na-Ascorbate (Sigma A7631-25G), 1 µM Alexa647 Azide (Thermo Fisher Scientific A10266) and $CuSO_4$ 0.1 M (Sigma C1297) for 30 minutes at room temperature in the dark, rotating. Cells were washed in DPBS/1%FBS/0.5% Tween 20 (Sigma P9416-100ML) for 10 minutes and then twice in cold DPBS/1% FBS. After 1 hour incubation in 300 µl of DPBS/1%FBS /DAPI 2.5 g/ml (Thermo Fisher Scientific D1306), the samples were analyzed using an LSR II FACS (BD). The data acquired have been analysed using Flowjo software and plotted in R 3.5.1.

Intra-cellular FACS staining for ^{HA}Rif1

After four days of OHT treatment, cells were collected and counted. $3 \cdot 10^6$ cells were fixed in 400 µl of DPBS (Thermo Fisher Scientific 14190094)/2% Paraformaldehyde (Sigma P-6148) for 10 minutes at room temperature shaking. Paraformaldehyde was then diluted at 0.2% and cells were washed in cold DPBS. After 2 minutes permeabilisation in 200 µl PBS-Triton X-100 0.1%, cells were incubated 5 minutes in saponin solution (COMPONENT E from kit C10424, Thermo Fisher Scientific) at room temperature and anti-HA antibody (Covance monoclonal HA.11 clone 16B12 #MMS-101R, RRID:AB_291262) was added 1:500. After 1 hour at room temperature rotating, cells were washed twice in DPBS/2% FBS, resuspended in 200 µl of saponin solution with anti-mouse ALEXA 647 1:1000 (Thermo Fisher Scientific A-21235, RRID:AB_2535804) and incubated for 1 hour rotating in the dark. After washing twice samples were resuspended in 400 µl of saponin solution with DAPI 2.5 g/ml (Thermo Fisher Scientific D1306) and analyzed on an LSR II FACS (BD). Data were processed on R version 3.5.1.

HiC

After four days of OHT treatment, cells were collected and counted. Cells were washed twice in cold DPBS and resuspended in full media. Samples were crosslinked for 10 minutes rotating at room temperature in 1% formaldehyde (10^6/ml). Crosslinking was stopped by adding glycine pH 5.0 at the final concentration of 0.2 M for 5 minutes at RT. Samples were washed twice in cold DPBS and pellets were snap frozen. 10^6 cells per sample were lysed in 10 mM Tris-HCl pH 8.0, 10 mM NaCl, 0.2% IGEPAL (Sigma, I3021) supplemented with protease inhibitor (Thermo Scientific, 78430) for 15 minutes on ice. Nuclei were washed twice in cold lysis buffer, resuspended in 50 µl of NEBuffer 3 (NEB, B7203) supplemented with 0.3% SDS and incubated at 62°C for 10 minutes. Diluting and quenching the SDS by adding 57.5 µl of NEBuffer 3 and 12.5 µl of 20% Triton X-100 (Sigma, 93443), samples were incubated at 37°C for 60 minutes. Nuclei were spun and incubated in 250 µl of 1× DpnII buffer with 600 U of DpnII restriction enzyme (NEB, R0543L) overnight at 37°C. Additional 200 U of DpnII were added to each sample the following day and incubated for further 2 hours.
After heat inactivation of DpnII, restriction fragments ends were filled by DNA polymerase I, Large (Klenow) Fragment (NEB, M0210), 0.8 U/µl of DNA, in 50 µl of 0.3 mM biotin-14-dATP (Thermo Fisher, 19524016), 0.3 mM dCTP/ dGTP/ dTTP for 1.5 hours at 37°C.

900 µl of ligation master mix were then add to the samples: 1.33x NEB T4 DNA ligase buffer (NEB, B0202), 1.1% Triton X-100, 1.33 mg of Bovine Serum Albumin and 2000 U of T4 DNA Ligase (NEB, M0202). Samples were incubated for 4 hours rotating. Nuclei were spun and resuspended in water and digested with proteinase K 1.2 mg/ml and 0.8% SDS at 55°C for 30 minutes. 130 µl of 5 M NaCl were added and samples were incubated at 65°C overnight. After ethanol precipitation, DNA was resuspended in 500 µl of 10 mM Tris-HCl pH8 and washed trice using the same buffer using Amicon filters (Millipore, UFC503096). Samples were diluted in 50 mM Tris pH 8.0, 0.1% SDS, 10 mM EDTA and sonicated to about 500 bp using a probe-based sonicator. Washes were then repeated as in the previous step. Biotinylated DNA was pulled down using 30 µl of 10 mg/ml Dynabeads MyOne Streptavidin T1 beads (Life technologies, 65602) in 10 mM Tris-HCl (pH 7.5); 1 mM EDTA; 2 M NaCl for 15 minutes at room temperature rotating. Beads were washed in TWB: 5 mM Tris-HCl (pH 7.5); 0.5 mM EDTA; 1 M NaCl; 0.05% Tween 20 for 2 minutes at 55°C twice, resupended in 20 µl 1× NEB T4 DNA ligase buffer, transferred to a new tube and incubated for 30 minutes at room temperature with 100 µl of: 1x NEB T4 DNA ligase buffer, 0.5 mM dNTPs, 50 U T4 PNK (NEB, M0201), 12 U T4 DNA polymerase I (NEB, M0203), 5 U DNA polymerase I, Large (Klenow) Fragment. After two washes in TWB at 55°C for 2 minutes, beads were transferred to 1× NEBuffer 2 (NEB, B7202) and moved to a new tube. Beads were then incubated at 37°C for 30 minutes in 100 µl of 0.9X NEBuffer 2, 0.5 mM dATP and 25 U Klenow exo minus (NEB, M0212). Beads were washed again as before and transferred to T4 ligation buffer. DNA was ligated for 2.5 hours with Illumina adaptors in 50 µl of the following reaction mix: 1X T4 ligation buffer, 1.2 µM Illumina adaptors, 1U T4 DNA ligase. Beads were washed once again with TWB as before, to be then resuspended and stored in 50 µl of 10 mM Tris-HCl (pH8).
Libraries were amplified in six parallel reactions using Illumina primers and 2 µl of beads per reaction after testing optimal amplification cycles. Size selection was performed on an agarose gel, isolating fragments between 300-800 base pairs (bp), followed by purification with QIAquick Gel Extraction Kit (Qiagen 28704). Each library was sequenced on one lane of Illumina Nex-seq 500 (75 bp paired end reads). FASTQ files were processed with the distiller pipeline (https://github.com/mirnylab/distiller-nf, DOI:10.5281/zenodo.2630563) to obtain *.cool* files used in downstream analyses. The customized scripts for the downstream analysis are available in the supplementary information. The original names of the cell lines that have been used for these experiments and that are included in the sequencing raw file names are: RFHF14 = Rif1-FH, 14 tgWT A7 = Rif1-TgWT 1, 14 tgWT G10 = Rif1-TgWT 2, 14 tgwt H4 = Rif1-TgWT 3, 14 ΔP F8 = Rif1-ΔPP1 1, 14 ΔP H1 = Rif1-ΔPP1 2, 14 ΔP H2 = Rif1-ΔPP1 3, ESC B = Rif1-WT 1, ESC 5:16 = Rif1-WT 2, ESC 5:3 = Rif1-WT 3, ESC 24 = Rif1-KO 1, ESC 15:10 = Rif1-KO 2, ESC 16:9 = Rif1-KO 3.

Protein extraction

Cells were washed twice in cold DPBS and resuspended in hypotonic buffer: 25 mM Tris-HCl (pH 7.4); 50 mM KCl; 2 mM $MgCl_2$; 1 mM EDTA, proteinase inhibitor (Roche, 5056489001) at the concentration of $20 \cdot 10^6$ cells/ml. Samples were incubated for 20 minutes on ice, washed twice with hypotonic buffer and resuspended in same volume of Benzonase buffer: 50 mM Tris-HCl (pH 8.0); 100 mM NaCl; 1.5 mM MgCl2; 10% Glycerol; proteinase inhibitor (Roche, 5056489001). After 3 cycles of snap freezing and thawing, samples were supplemented with 50 U/ ml of benzonase (Sigma, E1014) and incubated at room temperature for 25 minutes. 0.2% Triton X-100 was added and samples were incubated for 10 minutes at 4°C rotating. After

centrifugation, supernatant was collected and quantified by Bradford (Bradford 1976) (Biorad, 5000006). SDS-Page and Western Blot analysis were performed as in Foti et al. 2016, loading 40 µg of proteins per lane.

RNA extraction and qRT-PCR.

Total RNA was extracted using RNeasy kit (QIAGEN) according to manufacturer's instructions. cDNA synthesis was performed using RevertAid H Minus reverse transcriptase (Thermo Scientific) and qPCR was performed using the SYBR Green reaction mix (Roche) on a LightCycler 96 Instrument. Gene expression data was normalized against GAPDH and the relative RNA expression levels were calculated using the Ct (2^ΔΔCt) method.

3D-SIM and image analysis

Cells were split on a coverslip on the 4th day of tamoxifen treatment and after 5 hours were pulsed with 10mM BrdU for 15 minutes. After 2x washes in warm PBS, cells were chased for 3 hours in CO_2 pre-equilibrated, warm medium. After 2x washes in PBS, cells were fixed for 10 minutes in methanol free 3.7% formaldehyde. For immunostaining, fixed cells were permeabilized for 15 minutes in 0.5% TritonX-100/PBS, blocked for 30 minutes in 0.02% Tween 20/PBS/2% BSA, and stained with anti BrdU antibody (Biomol, Rockland, 600-401-C29, RRID:AB_10893609) for 60 min at 37 °C. Washes were performed in PBS/0.02% Tween. Immunostained cells mounted in Vectashield (Vector Laboratories) were used for super resolution imaging. Samples were acquired on a 3D-SIM Deltavision OMX V3 microscope (General Electric) equipped with a 100 × 1.4 oil immersion objective UPlanSApo (Olympus), 405 nm, 488 nm and 593 nm diode lasers and Cascade II EMCCD cameras (Photometrics). After acquisition, the 3D-SIM raw data were first reconstructed and corrected for colour shifts with the help of the provided software softWoRx 6.0 Beta 19 (unreleased). In a second step, a custom-made macro in Fiji (Schindelin, Arganda-Carreras et al. 2012) finalised the channel alignment and established composite TIFF stacks, that are subsequently used for image analysis.

Antibodies

Antigen	Source	Cat. #	Class	Use and dilution
HA	Covance	HA.11, 16B12	Monoclonal Mouse	WB 1:1000 IF 1:3000 FACS 1:3000
Rif1	Buonomo et al. 2009	1240	Polyclonal Rabbit	WB 1:3000
SMC1	Bethyl	A300-055A	Polyclonal Rabbit	WB 1:10000
BrdU	Biomol (Rockland)	600-401-C29	Polyclonal Rabbit	IF 1:300

Primers

Primer	**Sequence 5' – 3'**	**Reference**
MERVL F	atgggtccaggaatcaaggg	This paper
MERVL R	gcctctggagccaaaacttc	This paper
GAPDH F	tgtgagggagatgctcagtg	This paper
GAPDH R	atggccttccgtgttcctac	This paper

References

Bradford, M. M. (1976). "A rapid and sensitive method for the quantitation of microgram quantities of protein utilizing the principle of protein-dye binding." Anal Biochem **72**: 248-254.

Ryba, T., I. Hiratani, T. Sasaki, D. Battaglia, M. Kulik, J. Zhang, S. Dalton and D. M. Gilbert (2011). "Replication timing: a fingerprint for cell identity and pluripotency." PLoS Comput Biol **7**(10): e1002225.

Schindelin, J., I. Arganda-Carreras, E. Frise, V. Kaynig, M. Longair, T. Pietzsch, S. Preibisch, C. Rueden, S. Saalfeld, B. Schmid, J. Y. Tinevez, D. J. White, V. Hartenstein, K. Eliceiri, P. Tomancak and A. Cardona (2012). "Fiji: an open-source platform for biological-image analysis." Nat Methods **9**(7): 676-682.

Supplemental Information

Fig. S1 Generation of ESCs expressing RIF1-ΔPP1. Related to Fig. 1.

A. In $Rif1^{FH/flox}$ ESCs, the $Rif1^{FH}$ allele was targeted. The targeting construct allows knocking-in Rif1's codon-optimised cDNA (exons 8 to 36), either wild type or carrying the SAAA/RVSF ($Rif1^{\Delta PP1}$) mutations of the SILK and RVSF motifs, residues 2128–2131 and 2150–2153. The homology arms included in the construct to target the *Rif1* locus are shaded in grey. The targeted alleles are indicated in the figure as $^{FH}Rif1^{TgWT}$ or $^{FH}Rif1^{\Delta PP1}$ respectively. Splicing between genomic-encoded exon 7 and cDNA-encoded exon 8 allows expression of Rif1-TgWT or Rif1-ΔPP1 respectively. Restriction sites and probe used to identify by southern blot the correct insertion of the targeting construct in $Rif1^{FH}$ allele and not the $Rif1^{flox}$ allele are indicated. The map of $Rif1^{flox}$ allele indicating the expected sizes after restriction digest and Southern blot analysis is shown.
B. Southern blot confirmation of correct integration of the targeting constructs in the cell lines employed in this work.

Fig. S2 RIF1-ΔPP1's impact on the replication-timing program does not entirely recapitulate the consequences of RIF1 loss of function. Related to Fig. 2.

A. Percentage of 50kb-windows changing RT from Early-to-Late S-phase (EtoL, from a positive to a negative RT value), Early -to-Earlier (to Earlier, thus more positive value value of RT), from Late-to-Early (LtoE, from a negative to a positive RT value), and from Late-to-Later S-phase (to Later, thus more negative value of RT), over increasing thresholds.
B. Representative RT profile from one line per genotype at 1kb resolution.
C. Relative distribution of S-phase cells (EdU positive) between DNA contents corresponding to early, mid and late replication, as determined by DAPI quantitation (FACS). The average value of three independent clones with the same, indicated genotypes is shown. Average of three experiments. Error bars indicate standard deviations. *P* values are calculated using Kruskal–Wallis test.

Fig. S3 Classification of dynamic spatial distribution of replication foci in mESCs. Related to Fig. 2.

A. RIF1 dynamic distribution throughout cell cycle and S-phase substages classification. G1 and G2 cells are distinguished by the combination of EdU (red) and anti-histone H3 Ser10-phospho antibody staining (H3S10Ph, cyan). $Rif1^{FH/FH}$ (green) is visualized by immunofluorescence with the anti-HA mouse ascites 16B12. Spatial distribution of replication foci (EdU) was employed to divide S-phase into 6 substages. In blue, DNA staining (DAPI). The side lines indicate further grouping of S1, S2 and S3 as Early, S4 as Mid and S5, S6 as Late S-phase.
B. Number of replication forks per cell, for two independent biological replicates per genotype (except for Rif1-WT, where only one clone was analysed). The line represents the median values and the 95% confidence intervals. *P* value is calculated using Kruskal Wallis test. The forks were visualised by anti-BrdU staining and 3D-SIM image acquisition.

C. Boxplots showing the distribution of the number of replication forks per replication focus, from 1C. *P* values are calculated using t test. (0.05> *P* value >0.01 == *, 0.01 >= *P* value >0.001 == **, 0.001 >= *P* value >0.0001 == ***, *P* value < 0.0001 == ****)

Fig. S4 *Rif1* haploinsufficiency increases long-range chromatin contacts. Related to Fig. 3 and 4.

A. Median number of chromatin contacts (arbitrary units) between pair of TADs at increasing distances, measured as the number of TADs boundaries crossed by the interactions. Three biological replicas per genotype, except for Rif1-FH, are shown. Contacts are classified as *intra*-TADs, short-range (across the next-TAD boundary, and therefore inversely proportional to boundary strength), mid-range (between 2 and 30 TADs distance) and long-range (over 30 TADs apart). Median TAD's size=0.4Mb.
B. Mean of the median number of *in cis* interactions (arbitrary units) between two TADs of three independent biological replicates per genotype. Data are sub-divided into short, mid and long interactions as in A. *P* values are calculated using t-student test.
C. Representative distribution of the median number of *in cis* chromatin contacts per indicated position (arbitrary units) within the specified region of Chromosome 17, as in Fig. 3B. Heatmaps showing unsaturated signals.
D. Percentage of 50kb-windows changing compartment, calculated for increasing thresholds (ΔAB), as in Fig. 4D. However, here Rif1-KO is compared to Rif1-WT while Rif1-ΔPP1 is compared to Rif1-TgWT.

Figure 1

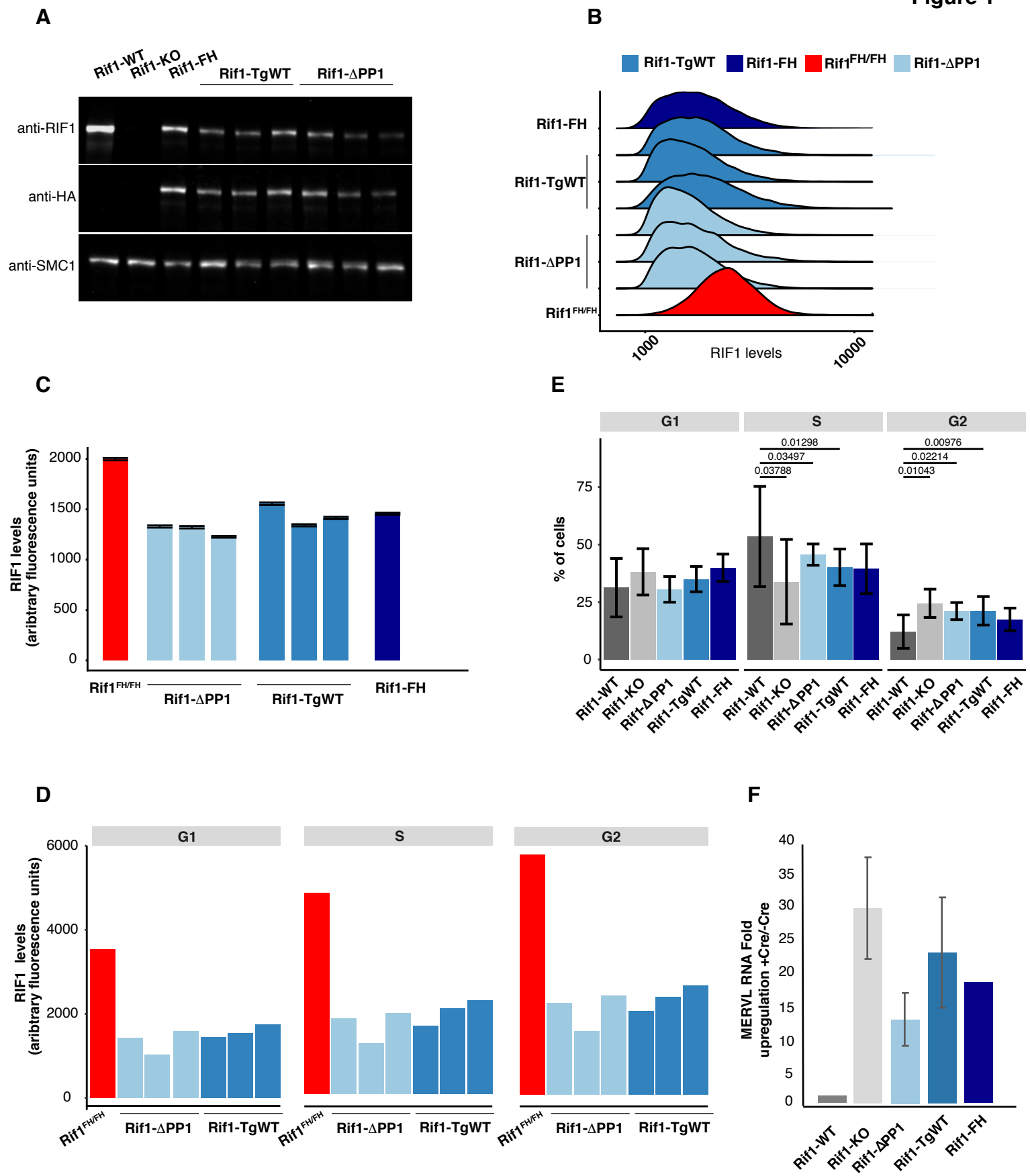

Figure 2

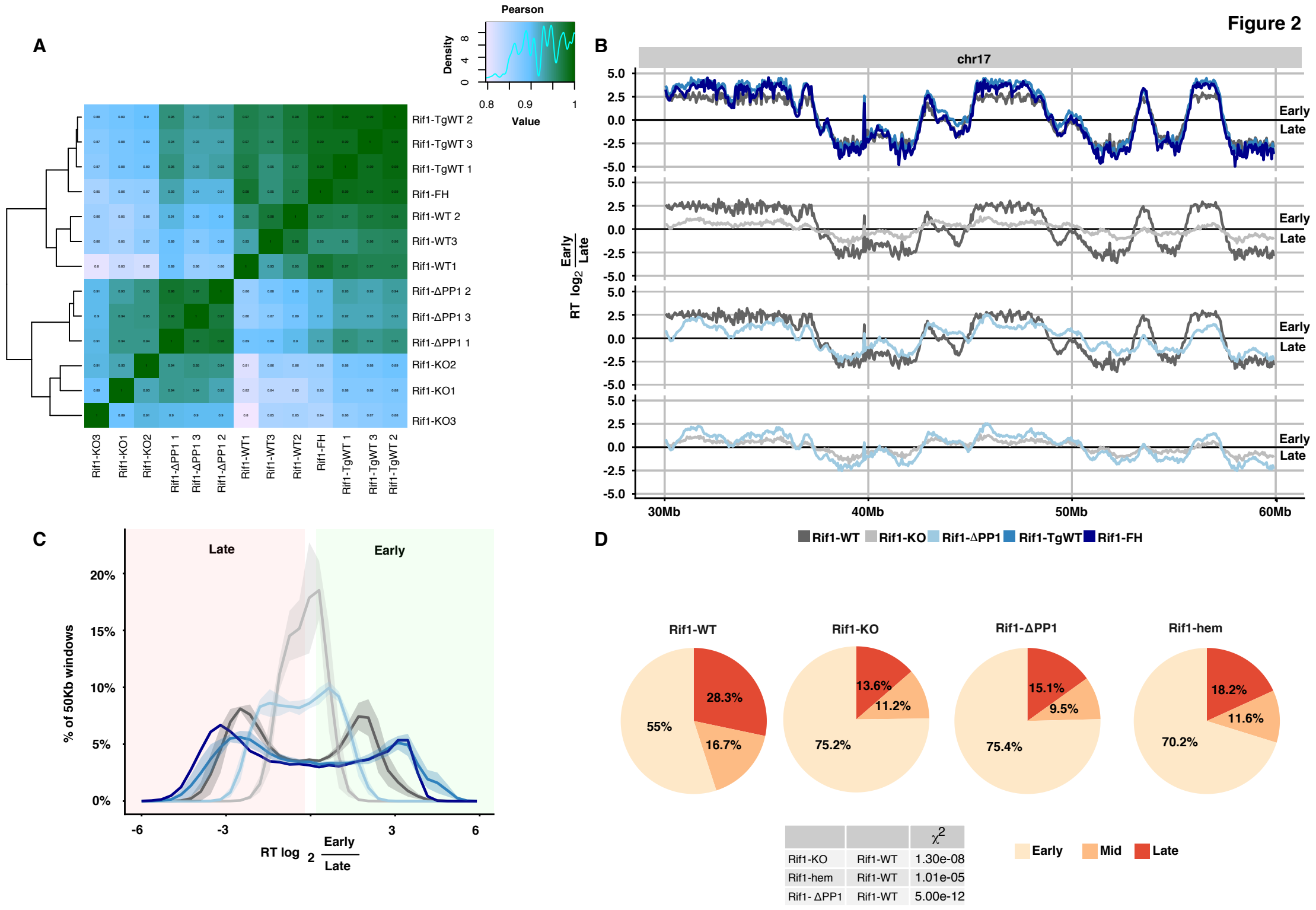

		χ^2
Rif1-KO	Rif1-WT	1.30e-08
Rif1-hem	Rif1-WT	1.01e-05
Rif1- ΔPP1	Rif1-WT	5.00e-12

Figure 3

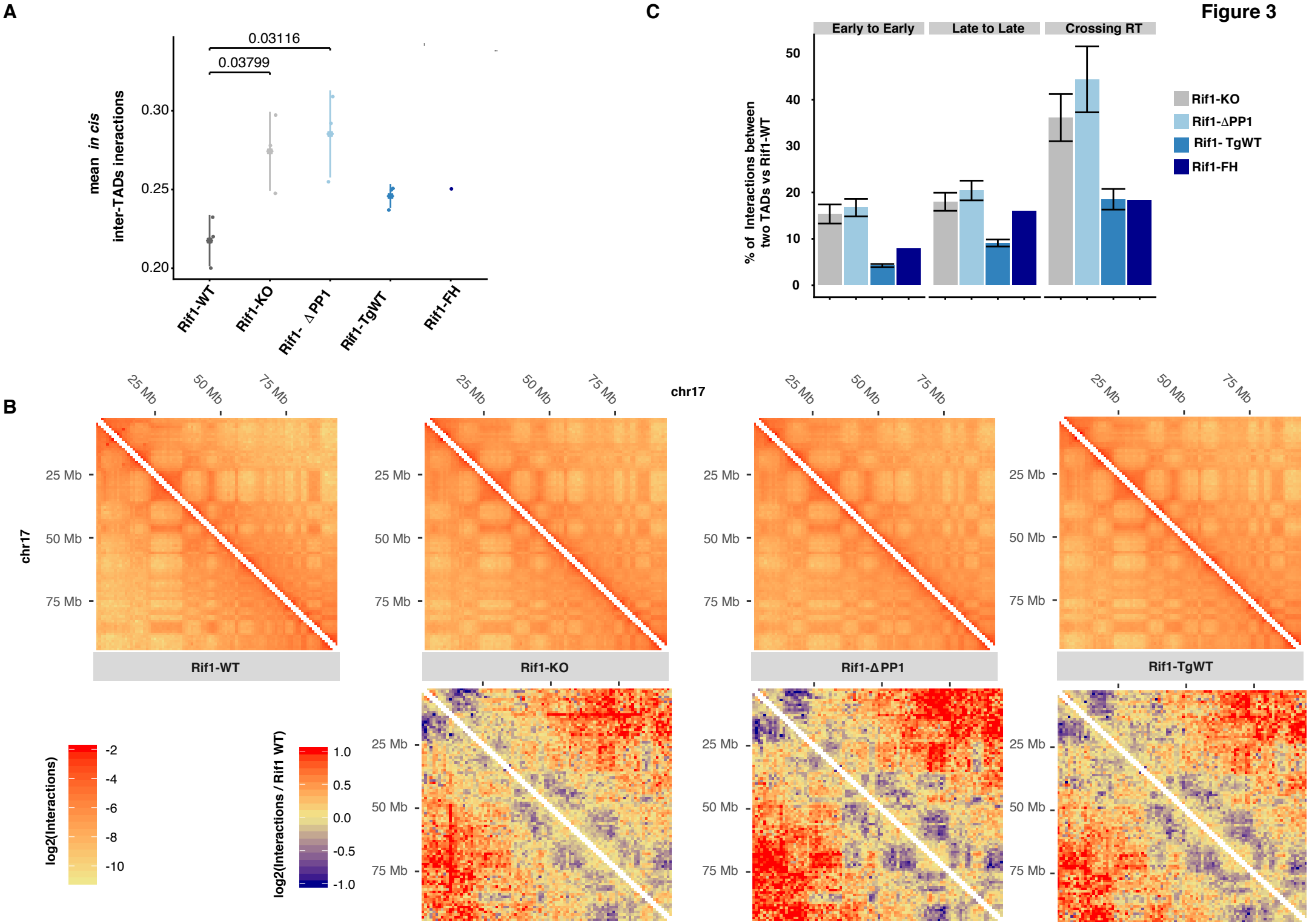
A
0.03116
0.03799
mean in cis inter-TADs ineractions
0.30
0.25
0.20
Rif1-WT
Rif1-KO
Rif1- ΔPP1
Rif1-TgWT
Rif1-FH
C
Early to Early
Late to Late
Crossing RT
% of Interactions between two TADs vs Rif1-WT
50
40
30
20
10
0
Rif1-KO
Rif1-ΔPP1
Rif1- TgWT
Rif1-FH
B
chr17
25 Mb
50 Mb
75 Mb
Rif1-WT
Rif1-KO
Rif1-ΔPP1
Rif1-TgWT
log2(Interactions)
-2
-4
-6
-8
-10
log2(Interactions / Rif1 WT)
1.0
0.5
0.0
-0.5
-1.0

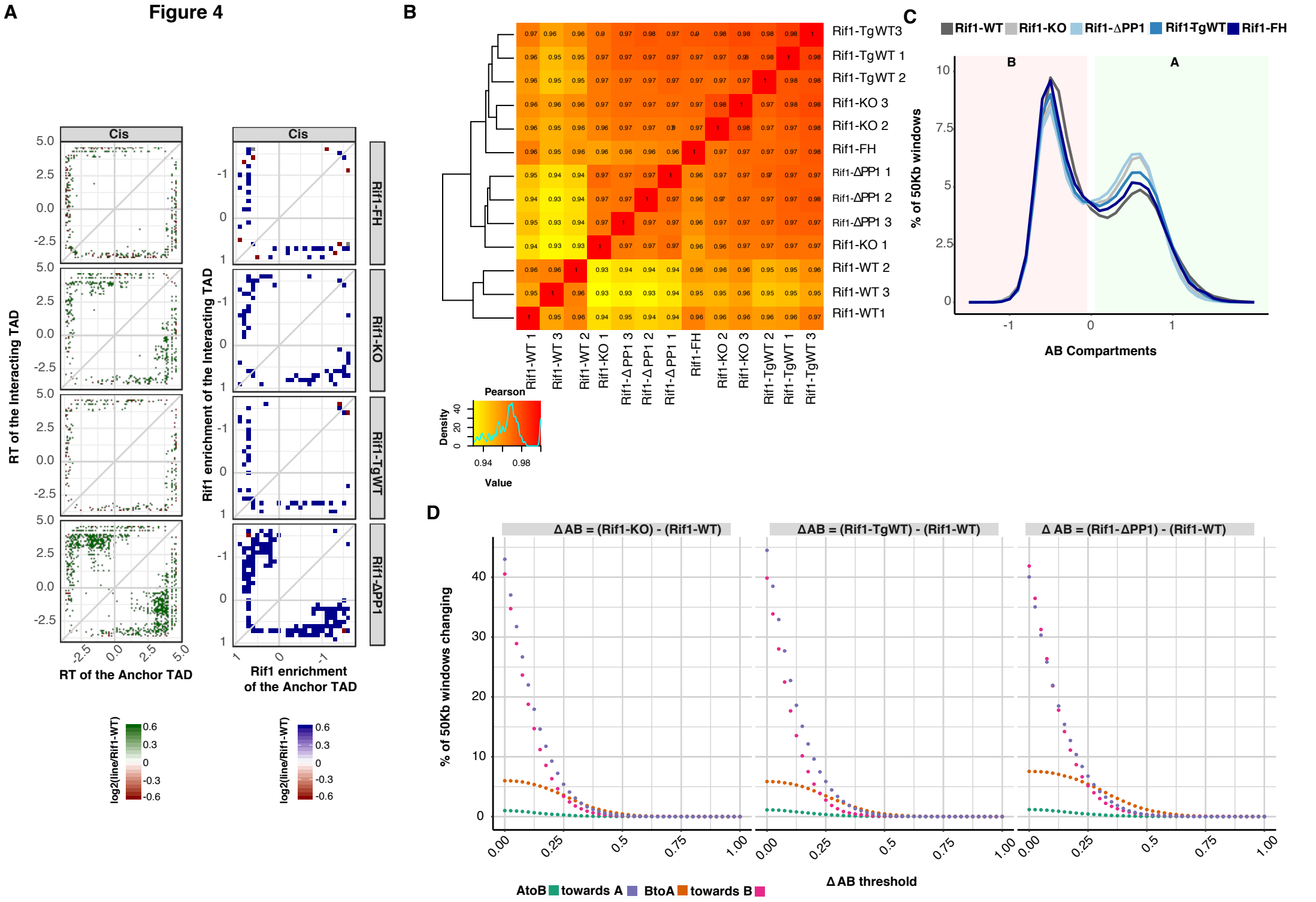
A
Figure 4
Cis
Cis
Rif1-FH
Rif1-KO
Rif1-TgWT
Rif1-ΔPP1
RT of the Interacting TAD
Rif1 enrichment of the Interacting TAD
RT of the Anchor TAD
Rif1 enrichment of the Anchor TAD
log2(line/Rif1-WT)
log2(line/Rif1-WT)
B
Rif1-TgWT3
Rif1-TgWT 1
Rif1-TgWT 2
Rif1-KO 3
Rif1-KO 2
Rif1-FH
Rif1-ΔPP1 1
Rif1-ΔPP1 2
Rif1-ΔPP1 3
Rif1-KO 1
Rif1-WT 2
Rif1-WT 3
Rif1-WT1
Rif1-WT 1
Rif1-WT 3
Rif1-WT 2
Rif1-KO 1
Rif1-ΔPP1 3
Rif1-ΔPP1 2
Rif1-ΔPP1 1
Rif1-FH
Rif1-KO 2
Rif1-KO 3
Rif1-TgWT 2
Rif1-TgWT 1
Rif1-TgWT 3
Pearson
Density
Value
C
Rif1-WT
Rif1-KO
Rif1-ΔPP1
Rif1-TgWT
Rif1-FH
B
A
% of 50Kb windows
AB Compartments
D
ΔAB = (Rif1-KO) - (Rif1-WT)
ΔAB = (Rif1-TgWT) - (Rif1-WT)
Δ AB = (Rif1-ΔPP1) - (Rif1-WT)
% of 50Kb windows changing
ΔAB threshold
AtoB
towards A
BtoA
towards B

Figure S1

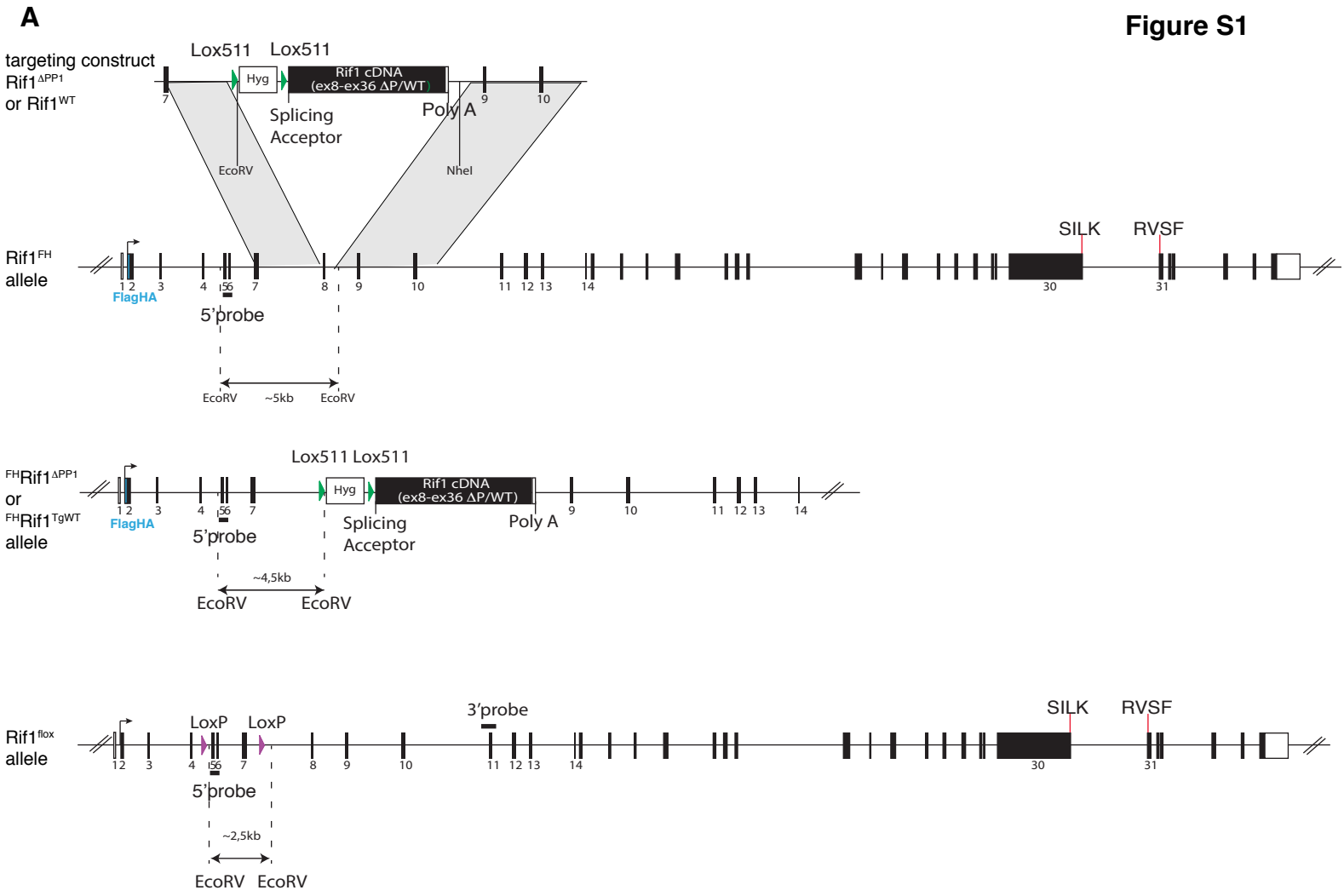

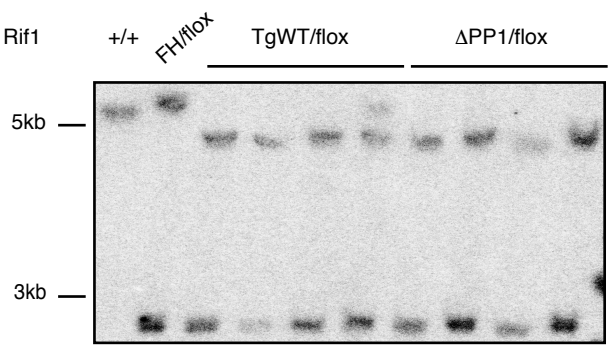

Figure S2

A

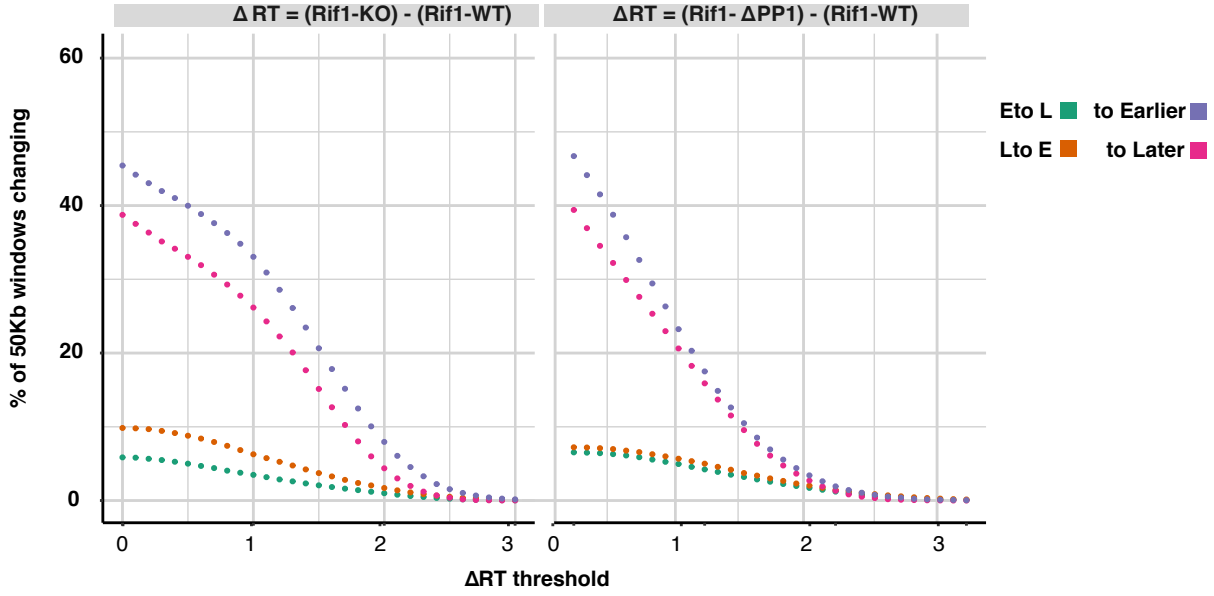

B

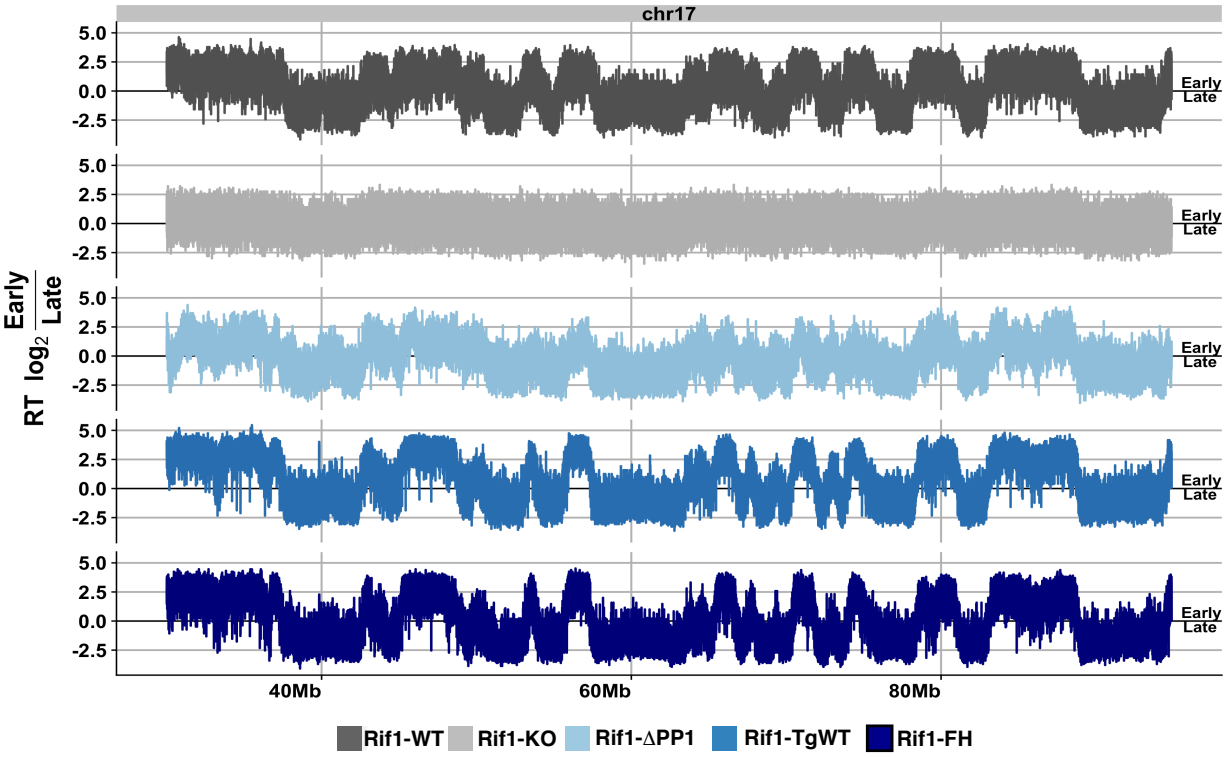

C

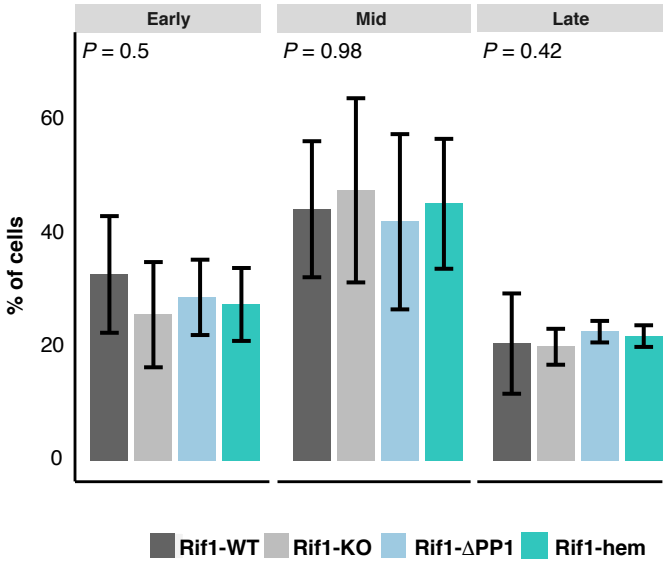

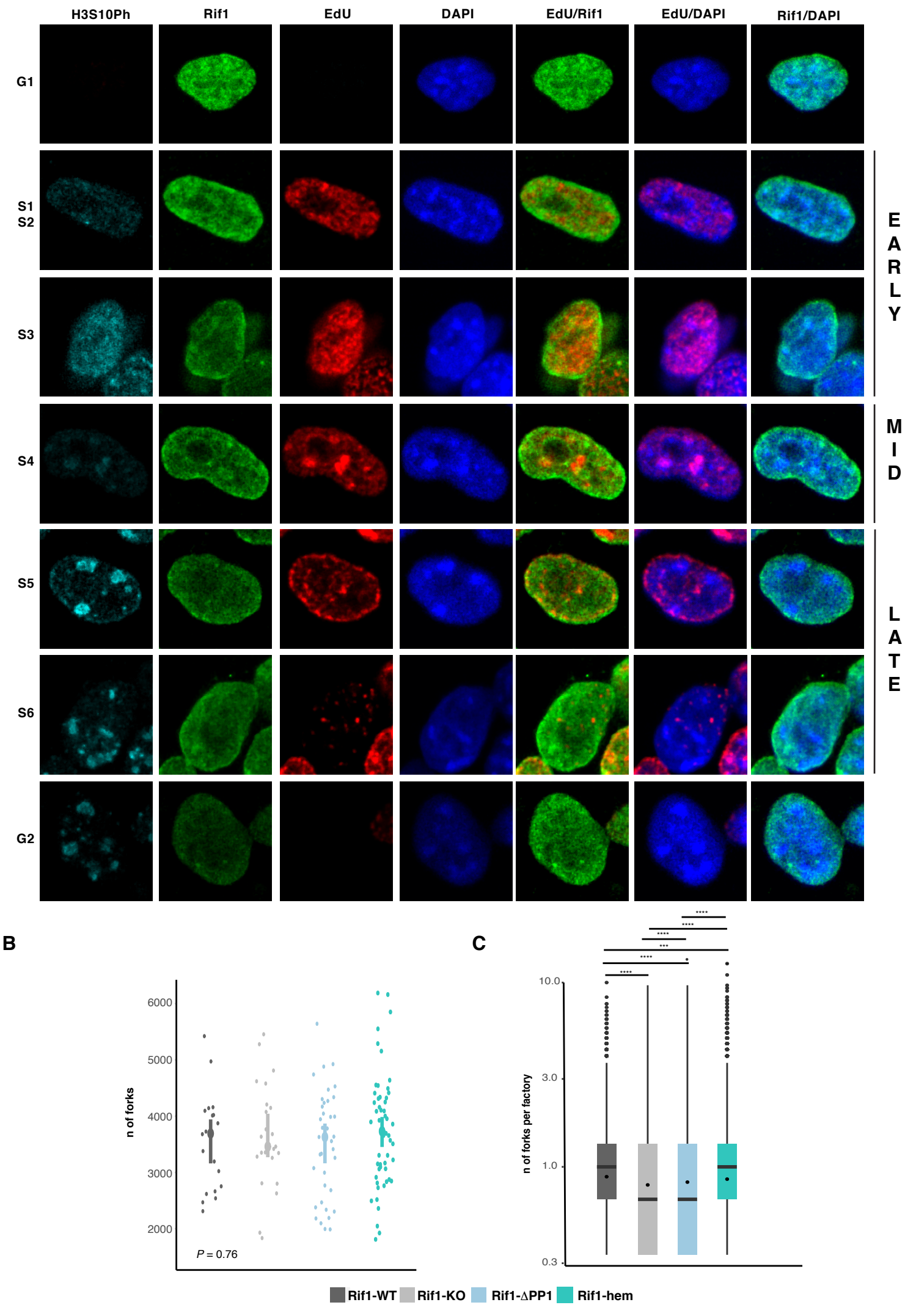

Figure S4

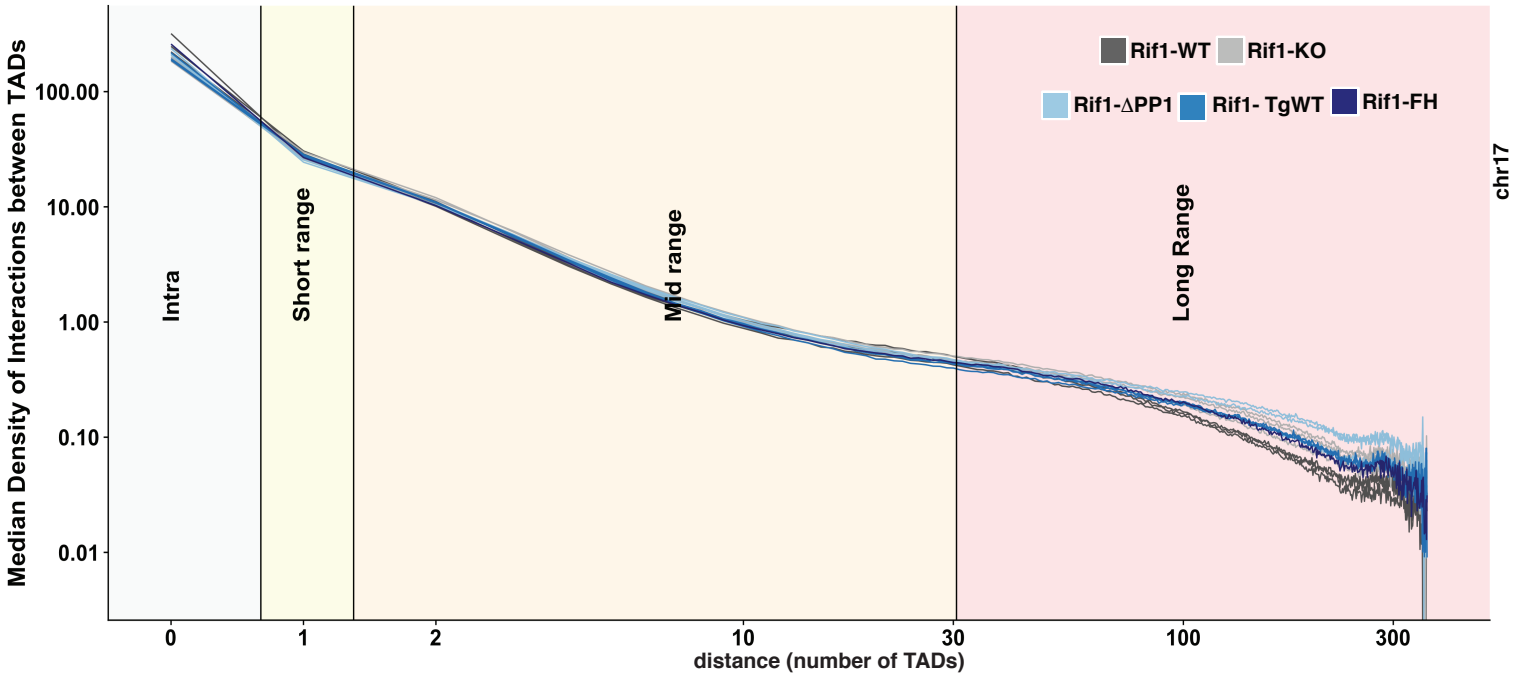
A
Median Density of Interactions between TADs
100.00
10.00
1.00
0.10
0.01
Intra
Short range
Mid range
Long Range
Rif1-WT
Rif1-KO
Rif1-ΔPP1
Rif1- TgWT
Rif1-FH
0
1
2
10
30
100
300
distance (number of TADs)

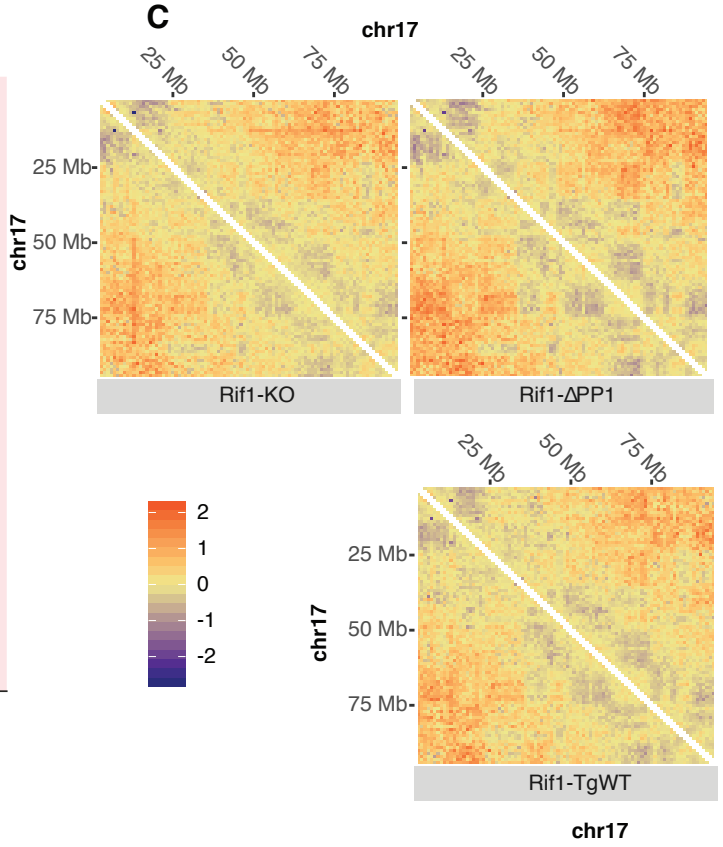
C
chr17
25 Mb
50 Mb
75 Mb
chr17
Rif1-KO
Rif1-ΔPP1
2
1
0
-1
-2
Rif1-TgWT
chr17

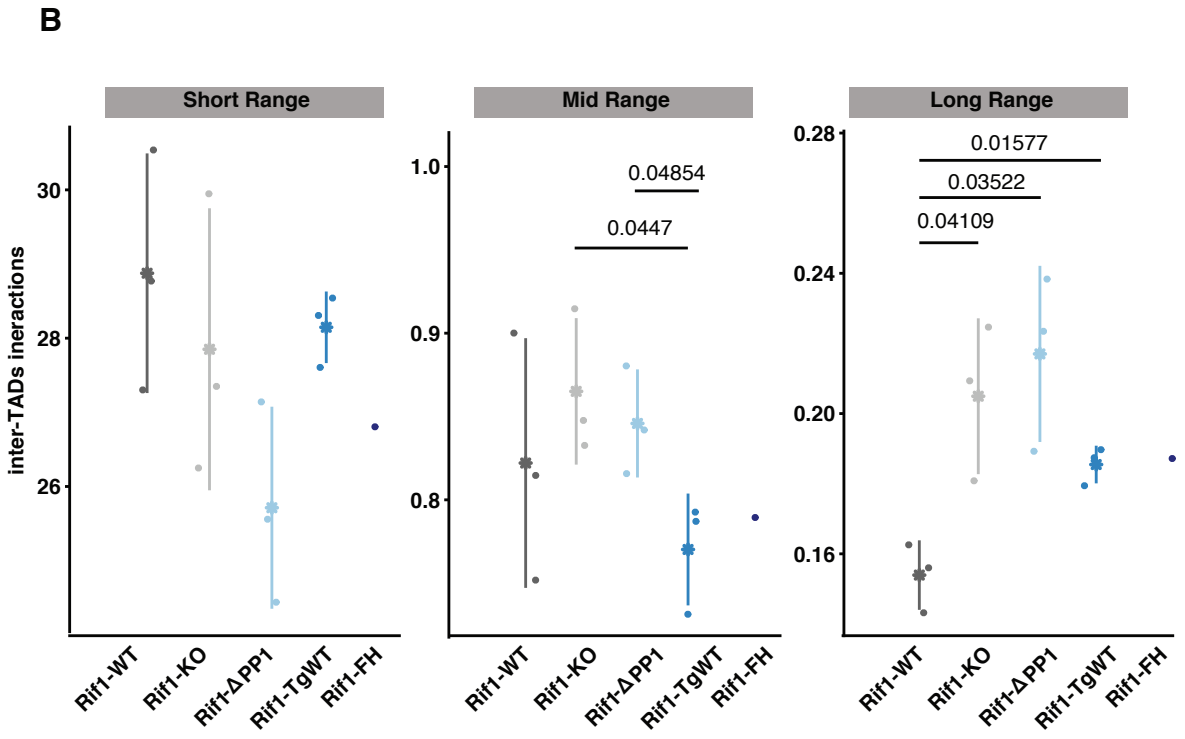
B
Short Range
Mid Range
Long Range
inter-TADs ineractions
30
28
26
1.0
0.9
0.8
0.28
0.24
0.20
0.16
0.04854
0.0447
0.01577
0.03522
0.04109
Rif1-WT
Rif1-KO
Rif1-ΔPP1
Rif1-TgWT
Rif1-FH

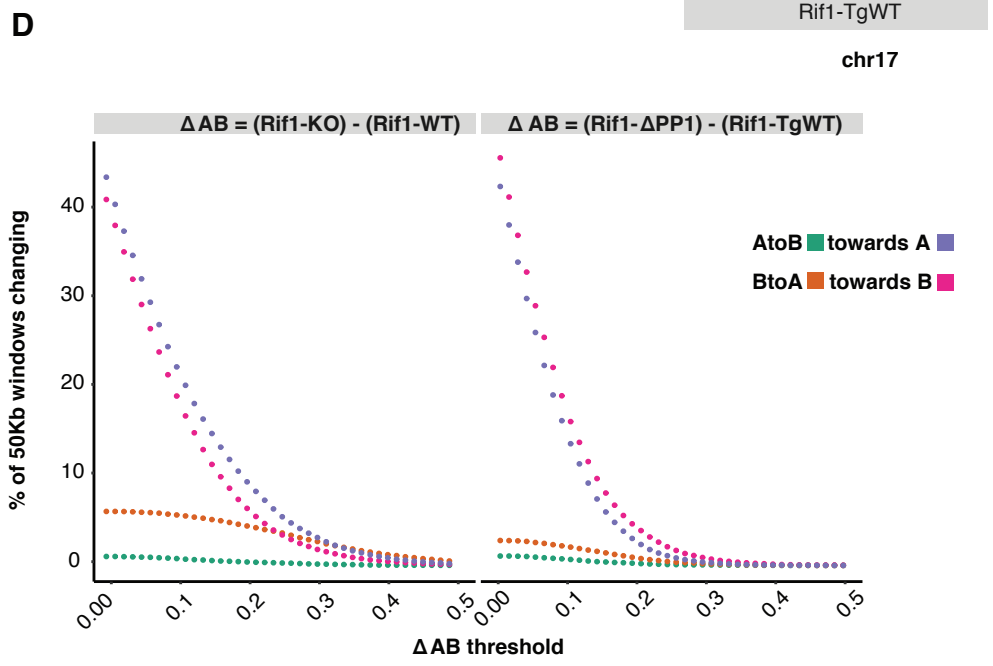
D
ΔAB = (Rif1-KO) - (Rif1-WT)
Δ AB = (Rif1-ΔPP1) - (Rif1-TgWT)
% of 50Kb windows changing
40
30
20
10
0
AtoB towards A
BtoA towards B
0.00
0.1
0.2
0.3
0.4
0.5
ΔAB threshold